Jisha Joseph “Self-assembly of structurally diverse phosphomolybdates: synthesis, structure and properties.” Thesis. Research and Post gradute Department of Chemistry, St. Thomas college (autonomous), University of Calicut, 2020.

CHAPTER III

Supramolecular isomerism in $\{P_2Mo_5\}$ cluster based solids

Summary

Self-assembly of molybdate and phosphate precursors in the presence of zinc ions and organic ligands *viz.* benzimidazole (*bimi*), 4-aminopyridine (4-*ap*) and pyrazole (*pz*) resulted in the crystallization of Strandberg cluster based solids {H*bimi*}$_5$[$HP_2Mo_5O_{23}$].$5H_2O$ (**3**), {H*bimi*}$_6$[$P_2Mo_5O_{23}$].H_2O (**4**), {4-H*ap*}$_4$[$H_2P_2Mo_5O_{23}$].$2H_2O$ (**5**), {4-H*ap*}$_5$[$HP_2Mo_5O_{23}$] (**6a**) and {H*pz*}$_6${Zn(*pz*)$_4$(H_2O)$_2$}[{Zn(*pz*)$_2$$P_2Mo_5O_{23}$}$_2$].$8H_2O$ (**7**) under hydrothermal condition. While, Solid **4** is the new supramolecular isomer of {H*bimi*}$_5$[$HP_2Mo_5O_{23}$].$5H_2O$ (**3**); Solids **5** and **6a** are new supramolecular isomers of {4-H*ap*}$_6$[$P_2Mo_5O_{23}$].$5H_2O$ (**6b**) which was reported earlier in literature. Under our reaction conditions, while pyrazole readily formed complex with zinc centers to form a derivatized Strandberg-type cluster; benzimidazole and 4-aminopyridine formed only organic-inorganic hybrid solids **3-6a**. The chapter, therefore, provides a rationale for the formation of Solids **3-6a** in terms of the reaction conditions. In addition, supramolecular isomerism in 4-aminopyridine based {P_2Mo_5} cluster anions varies due to the extent of protonation on the cluster anion. Therefore, the extent of protonation on cluster anion and the nature of the organic ligands on the optical band gap energies (E_g) of the synthesized solids were investigated.

III.1. Introduction

Designing polyoxometalates (POMs) through the self-assembly of entirely different counterparts is of great interest on account of their structural versatility and emerging applications. Strandberg-type phosphomolybdates (PMOs) are an important sub-family of POMs which plays a vital role in this area of research. A number of {P_2Mo_5} cluster based PMO solids with or without the incorporation of metal ions have been reported in literature [1-4]. The main synthetic methodologies adopted for crystallization of {P_2Mo_5} cluster based solids are solvent evaporation and hydrothermal synthesis [5,6]. While synthetic parameters such as temperature and pH of the reaction medium dictate the formation on PMO cluster anion [7-9]; selection of metal centers (for example, transition or rare earth metal ions) and organic ligands can induce structural features such as aggregation of water clusters, interpenetration and supramolecular isomerism [10-12].

As discussed in Chapter I, according to Moulton and Zaworotko, "Supramolecular isomerism in this context is the existence of more than one type of network superstructure for the same molecular building blocks and is therefore related to structural isomerism at the molecular level. In other words, the relationship between supramolecular isomerism and molecules is similar to that between molecules and atoms." [13]. With respect to PMO cluster based solids, there are only limited examples of supramolecular isomers based on {P_2Mo_5} cluster anion. Therefore, in the present chapter, an attempt has been made to crystallize supramolecular isomers based on {P_2Mo_5} cluster in the presence of zinc chloride and ligands *viz.* benzimidazole (*bimi*), 4-aminopyridine (4-*ap*) and pyrazole (*pz*). The synthesis under hydrothermal condition resulted in four new {P_2Mo_5} cluster based solids. While, the solids **4** and **5** & **6a** are new supramolecular isomers of previously reported

hybrid solids {H*bimi*}$_5$[$HP_2Mo_5O_{23}$].5H_2O [14] and {4-H*ap*}$_6$[$P_2Mo_5O_{23}$].5H_2O [15] respectively; {H*pz*}$_6${Zn(*pz*)$_4$(H_2O)$_2$}[{Zn(*pz*)$_2$$P_2Mo_5O_{23}$}$_2$].8$H_2O$, **7** can be considered as a pseudopolymorph of previously reported solid (*pz*)[{Zn(*pz*)$_3$}$_3${$P_2Mo_5O_{23}$}].2H_2O [16]. The chapter highlights the structural differences in the supramolecular isomers; and the effect of supramolecular isomerism in {P_2Mo_5} cluster based solids and nature of ligands on the optical band gap energy (E_g) of the synthesized solids. A comparative study has been done on the effect of protonation of the cluster anion with same organic ligands on the band gap energy.

III.2. Experimental Section

III.2.1. Synthesis

A mixture of zinc chloride ($ZnCl_2$, 0.075 g, 0.55 mmol, Aldrich, 98%), benzimidazole (3.3 mmol, Aldrich, 98%) and sodium molybdate (Na_2MoO_4.2H_2O, 0.40 g, 1.65 mmol, Merck, 99%) was taken in 6 ml of distilled water, sealed in a 10 ml Teflon lined stainless steel container and heated at 150^{o}C for three days. The initial pH was adjusted using 1 M orthophosphoric acid. After slow cooling to room temperature, the white crystals of **3** (refer Scheme III.1) were washed with water and acetone and allowed to dry in air. The same procedure was repeated for the synthesis of solids **4-7** using benzimidazole, 4-aminopyridine and pyrazole. The same molar ratio was used for the synthesis **4**, however the molar ratio of Mo:Zn:ligand was adjusted to 1:1:6 for **5** and **6a** and 3:1:6 for **7**. The Solid **6b** was reproduced as reported in literature [15]. The yield of solids was found to be 70-75% based on Mo.

Interestingly, Solid **3** was synthesized by Z. Que *et. al*. via solvent evaporation technique using water-alcohol solution of $Na_2MoO_4.2H_2O$ and *bimi* in the molar ratio 1:0.73 [14]. However, synthesis of **3** under hydrothermal conditions has not been reported so far.

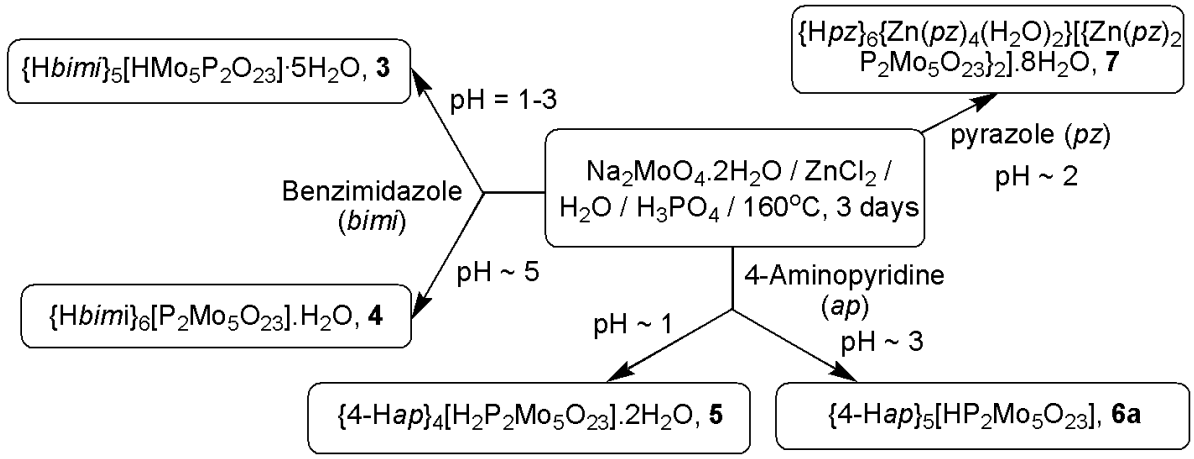

Scheme III.1. Scheme showing the experimental procedure to crystallize solids **3**-**7**.

III.2.2. Characterization

The solids were characterized using single crystal X-ray diffraction, powder X-ray diffraction, fourier transform infrared spectroscopy and thermogravimetric analysis. Band gap energy calculations were done using data collected from UV-Vis spectrophotometer as discussed under Section II.2.2 in Chapter II. The crystal and refinement data for solids **4-6** have summarized in Table III.1. The data for solid **7** will be discussed in Chapter IV along with other metal pyrazole complex incorporated {P_2Mo_5} cluster based solids.

III.3. Results and Discussion

The solids **3-6** are based on {P_2Mo_5} cluster anion and its structure has been discussed under Section II.3 in Chapter II.

Table III.1. Crystal and Refinement Data for Solids **4**-**6a**.

	4	**5**	**6a**
Formula	$C_{42}H_{42}Mo_5N_{12}O_{24}P_2$	$C_{20}H_{28}Mo_5N_8O_{25}P_2$	$C_{25}H_{35}Mo_5N_{10}O_{23}P_2$
Formula weight, g	1640.52	1322.14	1385.27
T (K)	298	298	296
Space Group	*P* $2_12_12_1$	P2_1/*c*	*P* 2_1/m
a, Å	10.7210(12)	19.858(5)	8.7972(18)
b, Å	14.7139(17)	11.326(3)	19.266(4)
c, Å	35.271(4)	17.957(4)	13.190(3)
α, °	90	90	90
β, °	90	105.289(4)	91.58(3)
γ,°	90	90	90
V, Å^3	5563.8(11)	3895.7(17)	2234.7(8)
Z	4	4	2
d_{calc}, g·cm^{-3}	1.959	2.254	2.059
$\mu_{MoK\alpha}$, cm^{-1}	1.247	1.749	1.528
λ (Å)	0.71073	0.71073	0.71073
$R_1(I>2\sigma I)$, WR_2(all)	0.0856, 0.1718	0.0662, 0.1172	0.0568, 0.1471
GOF	1.364	1.323	1.114

III.3.1. Crystal structure of 3

The crystal structure of **3** consists of monoprotonated cluster {HP_2Mo_5}, {H*bimi*}$^+$ cations and lattice water molecules. The protonation of only one of the phosphate groups was confirmed using Bond Valence Sum (BVS) calculations [17]. Crystal structural analysis revealed that N–H...O interactions aggregate {HP_2Mo_5} cluster anions and {H*bimi*}$^+$ cations to form a dimeric unit as shown in Figure III.1 (also refer Table III.2). These dimeric units are connected by {N1N3} moiety to form ladder-like 1-D chains which propagate along *a* axis. The lattice water molecules *viz*. O2W, O3W, O4W and O5W form a terameric unit which links the 1-D chains to form a 3-D supramolecular assembly (Figure III.1c, Table III.3). The packing of {H*bimi*}$^+$ moieties in **3** is reinforced by CH…π and π…π interactions as shown in Figure III.2. The crystal structure of **3** was earlier reported by Qu *et. al*. [14] as a 3-D supramolecular structure stabilized through electrostatic attraction, H-bonding and π...π interactions between {HP_2Mo_5} polyanion, {H*bimi*}$^+$ moieties and lattice water molecules.

Table III.2. H-bonding interactions in **3**.

D–H…A	D–H (Å)	H…A (Å)	D…A (Å)	∠ D–H…A (°)
N1-H1C…O3	0.775(47)	1.86(5)	2.617(5)	165.35(489)
N3-H3C…O13	0.753(61)	2.023(59)	2.760(5)	166.03(610)
N4-H4C…O2W	0.928(51)	1.795(52)	2.704(7)	165.84(465)
N6-H6C…O9	0.796(57)	2.023(56)	2.799(5)	164.53(567)
N7-H7C…O3	0.904(55)	1.979(54)	2.704(5)	136.18(477)
N9-H9D…O7	0.895(41)	1.837(44)	2.685(5)	157.30(342)
N12-H12C…O1W	0.804(54)	1.950(54)	2.734(6)	164.64(538)
N13-H13C…O22	0.821(58)	2.129(57)	2.864(5)	149.08(537)
N15-H15C…O10	0.780(47)	1.942(48)	2.718(5)	172.92(489)

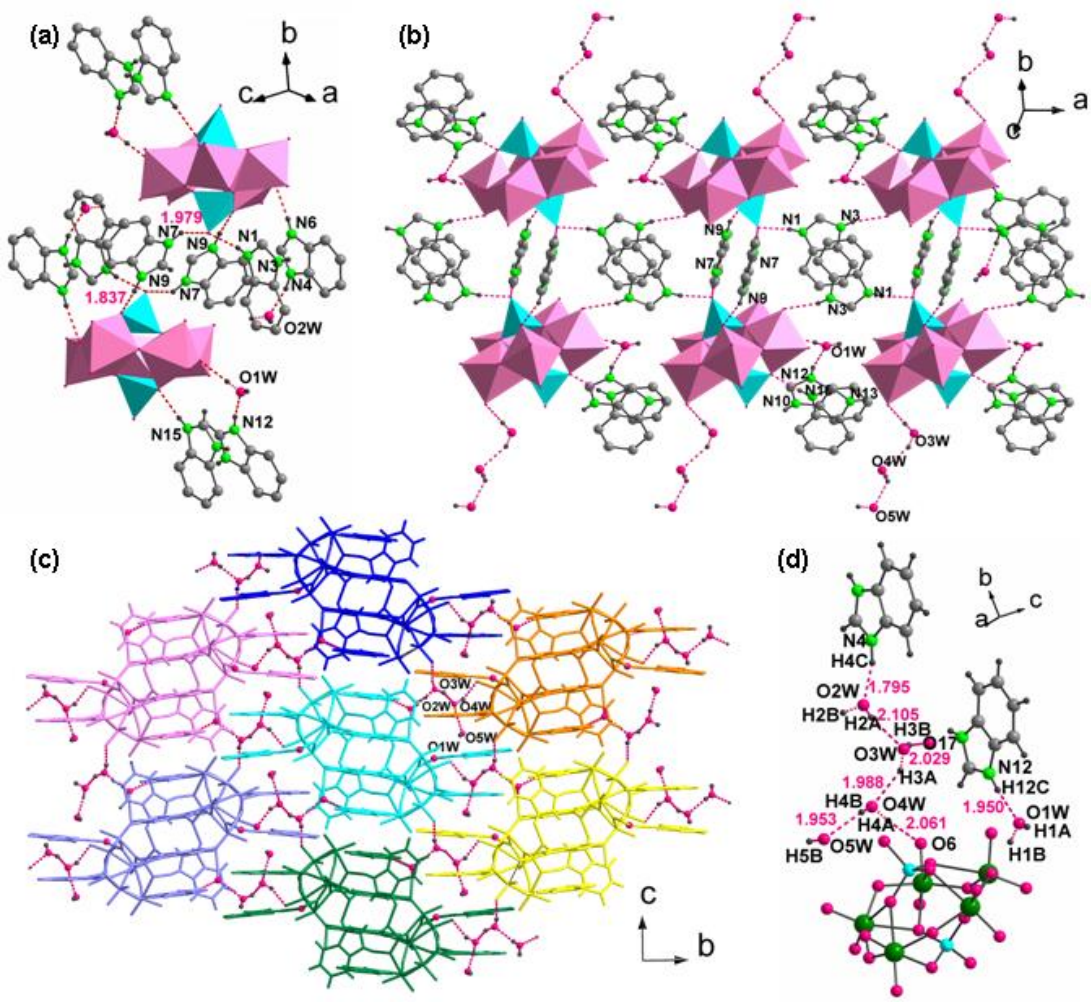

Figure III.1. (a) {HP_2Mo_5} anion shows extensive H-bonding interaction with the five {H*bimi*}$^+$ moieties, of which {N7N9} unit connects two {HP_2Mo_5} units to form a dimeric unit. For clarity only hydrogen atoms involved in N-H…O interactions (dashed red lines) have been shown in the figure. (b) The dimeric units are connected by {N1N3} moiety to form ladder-like 1-D chains propagating along *a* axis ({N4N6} moiety and lattice water molecule, O2W have been omitted). (c) View along *a* axis showing the connection between one 1-D chain (depicted in cyan color) with six others. The packing of chains is facilitated by water tetramer consisting of O2W, O3W, O4W and O5W. (d) H-bonding interactions exhibited by lattice water molecules.

Table III.3. H-bonding interactions in water tetrameric unit of **3**.

D–H…A	D–H (Å)	H…A (Å)	D…A (Å)	∠ D–H…A (°)
O2W-H2A…O3W	0.740(65)	2.105(66)	2.827(6)	165.13(705)
O3W-H3A…O4W	0.898(44)	1.988(57)	2.786(9)	147.30(398)
O4W-H4B…O5W	0.908(68)	1.953(72)	2.666(10)	134.19(486)

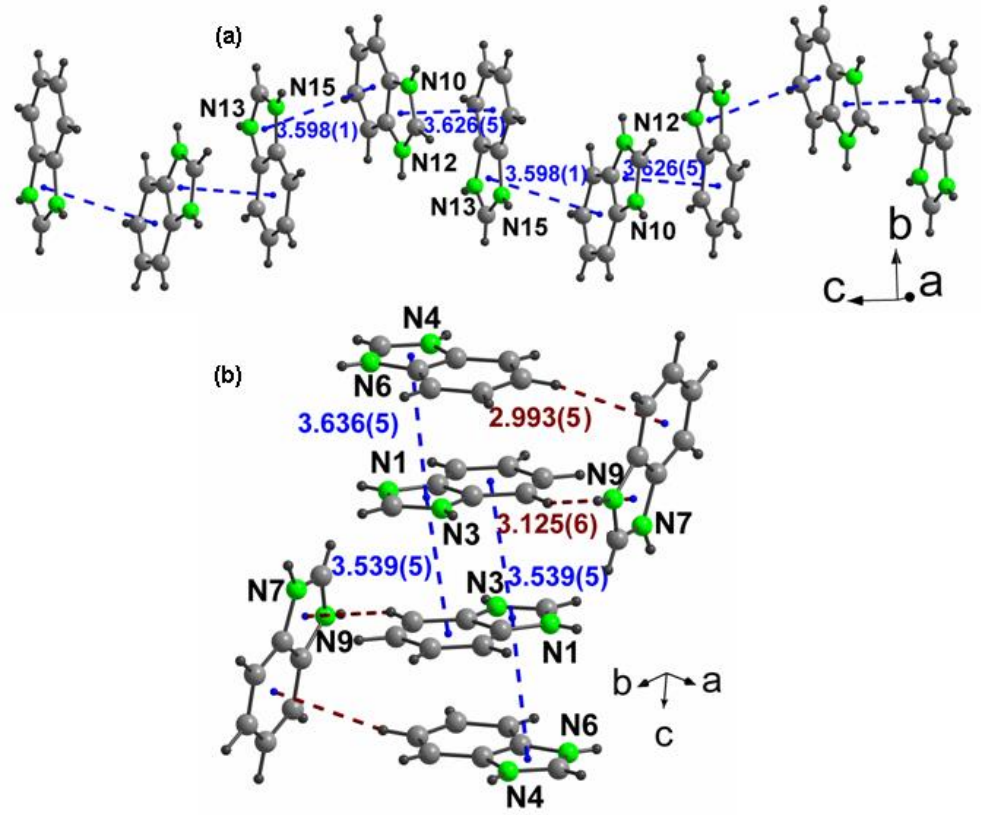

Figure III.2. (a) π…π interactions between {N10N12} and {N13N15} moieties. (b) CH…π and π…π interactions between {N1N3}, {N4N6} and {N7N9} moieties forming a hexameric unit. CH…π and π…π interactions have been shown in dashed brown and blue lines respectively.

III.3.2. Crystal structure of 4

Unlike **3**, the crystal structure analysis of **4** suggested the presence of one {P_2Mo_5} cluster anion, six {H*bimi*}$^+$ cations and one lattice molecule per asymmetric unit (refer Figure III.3). Of the six {H*bimi*}$^+$ moieties, H-bonding interactions mediated by {N5N6} link neighboring {P_2Mo_5} cluster anions to form 1-D chains which propagate along *a*-axis. The other four {H*bimi*}$^+$ moieties {N3N4}, {N7N8}, {N9N10} and {N11N12} exhibit extensively H-bonding interactions with the {P_2Mo_5} cluster anion. The 1-D chains are further connected through H-bonding interactions mediated by {N7N8} moieties to form 2-D corrugated sheet. N11-H11…O3 (2.019(10) Å) interactions between neighboring 2-D corrugated sheets facilitates the crystal packing in **4**. The packing of 2-D sheets results in the formation of voids which are occupied by the sixth benzimidazole moiety *viz.* {N1N2} along with the lattice water molecule, O1W (refer Figure III.3d). CH…π interactions also play a crucial role in crystal packing of **4**. While, three of the {H*bimi*}$^+$ moieties *viz.* {N5N6}, {N7N8} and {N9N10} are linked to each other though CH…π interactions; {N3N4} and {N11N12} form a dimer which further reinforce the H-bonding in 1-D chains of **4** (Figure III.4). In addition, the packing of 1-D chains to form 2-D corrugated sheets is favored by CH…π interactions exhibited by {N7N8} moieties (Figure III.5, also refer Table III.4 and III.5). It is noteworthy that **4** is the first supramolecular isomer of {H*bimi*}$_5$[$HP_2Mo_5O_{23}$].5H_2O reported by Qu *et. al.* [14].

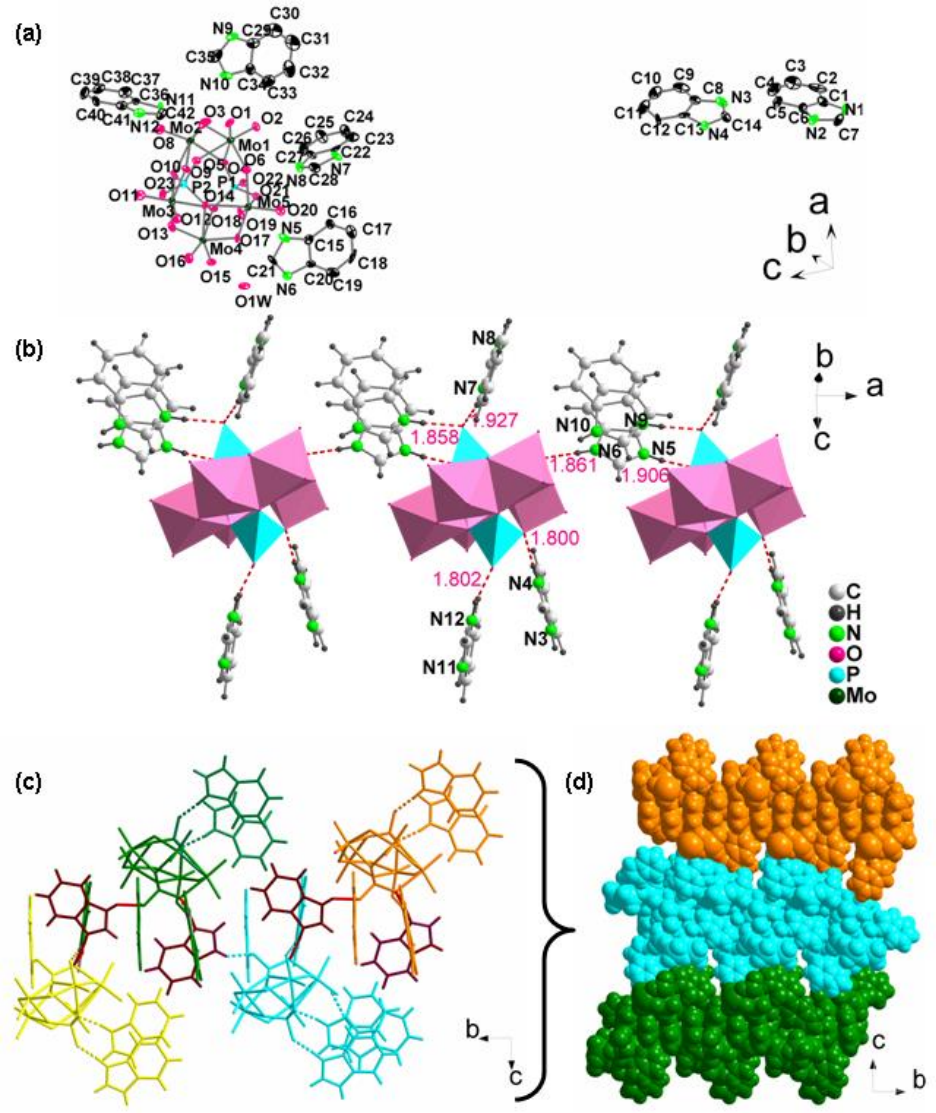

Figure III.3. (a) ORTEP view of **4**. The hydrogen atoms have been omitted for clarity. (b) 1-D chains formed via H-bonding interactions (shown in dashed red lines) mediated by protonated {N5N6} moieties. (c) NH…O interactions mediated by {N7N8} moiety (shown in brown color) link neighboring 1-D chains to form a 2-D corrugated sheet. The connection between four of these 1-D chains depicted in yellow, cyan, green and orange is shown herein. (d) View along *a* axis showing the crystal packing of 2-D corrugated sheets. The voids seen in figure are occupied by the sixth protonated benzimidazole moiety {N1N2} along with lattice water molecule, O1W.

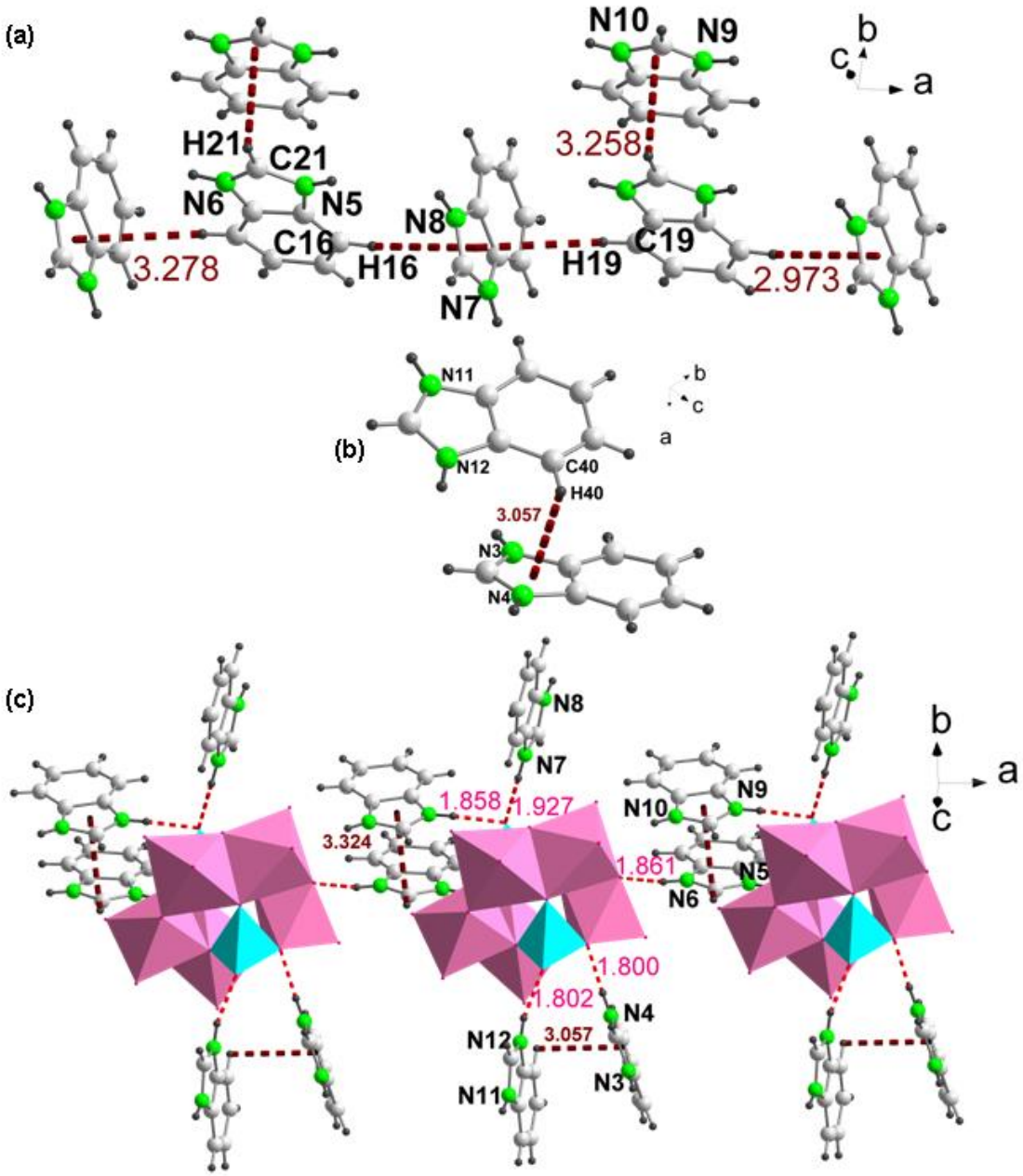

Figure III.4. (a) While three of the {H*bimi*}$^+$ moieties *viz.* {N5N6}, {N7N8} and {N9N10} are linked to each other though CH…π interactions (shown in dashed brown color); {N3N4} and {N11N12} merely form a dimer as seen in (b). (c) The H-bonding in 1-D chains of **4** is reinforced through CH…π interactions.

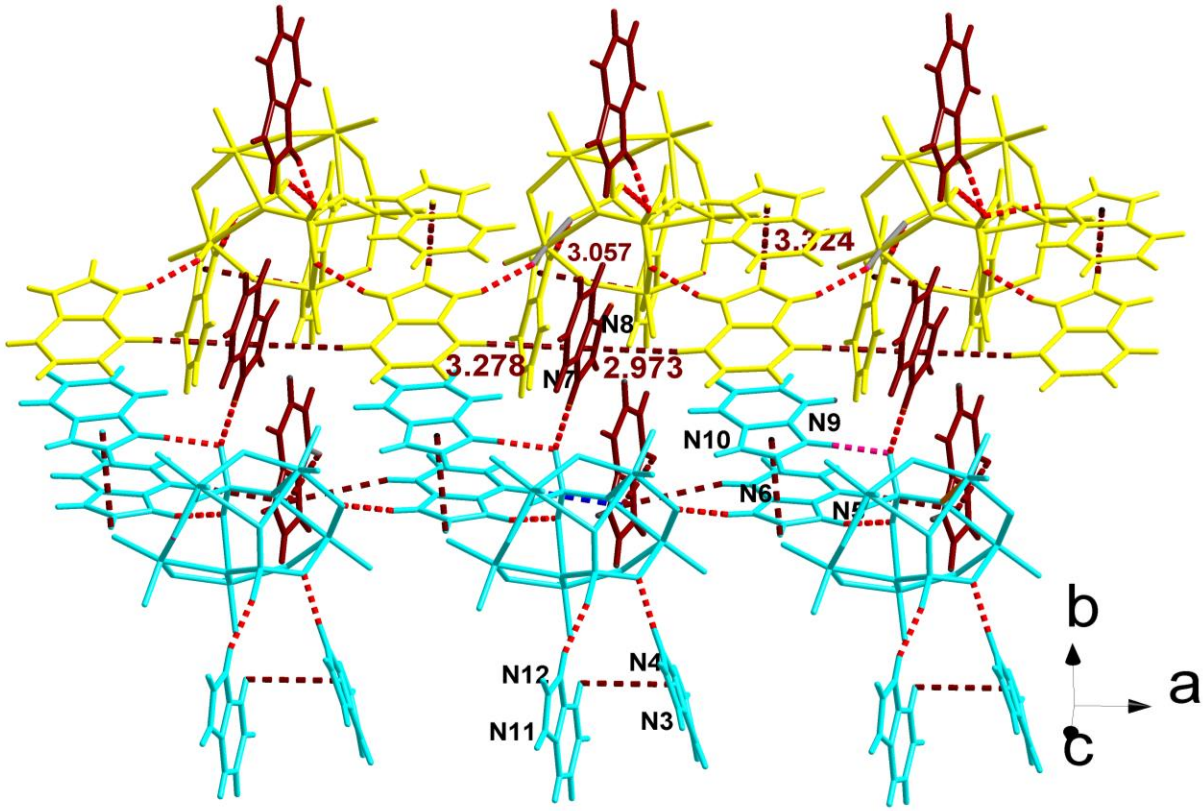

Figure III.5. The packing of 1-D chains is also facilitated through CH…π interactions. CH…π interactions mediated by {N7N8} moieties (shown in brown color) favors the crystal packing in **4**. Two neighboring 1-D chains are shown here in blue and yellow color. The dashed red lines represent H-bonding interactions.

Table III.4. H-bonding interactions in **4**.

D–H…A	D–H (Å)	H…A (Å)	D…A (Å)	∠ D–H…A (°)
N1-H1…O10	0.858(14)	2.255(8)	3.010(16)	146.86(96)
N2-H2…O1W	0.860(14)	1.903(11)	2.734(18)	162.12(98)
C7-H7A…O23	0.929(18)	2.163(10)	2.955(20)	142.66(11)
N3-H3…O11	0.861(14)	2.259(10)	3.012(18)	146.02(10)
N3-H3…O13	0.861(14)	2.084(11)	2.773(18)	136.58(98)
N4-H4…O5	0.860(11)	1.800(9)	2.653(14)	171.06(75)
N5-H5…O21	0.859(11)	1.906(8)	2.732(14)	160.57(79)
N6-H6…O2	0.860(13)	1.861(10)	2.695(16)	162.99(92)
C21-H21…O15	0.932(14)	2.332(11)	3.234(18)	162.89(91)
N7-H7…O22	0.860(12)	1.927(7)	2.700(14)	148.91(81)
N8-H8…O21	0.860(14)	1.952(8)	2.780(16)	161.08(94)
N9-H9…O22	0.859(13)	1.858(9)	2.697(15)	164.91(90)
N10-H10…O3	0.859(15)	2.353(10)	3.075(19)	141.98(10)
N10-H10…O7	0.859(15)	2.305(10)	3.052(18)	145.59(10)
N11-H11…O3	0.861(11)	2.019(10)	2.815(16)	153.22(79)
N12-H12…O23	0.861(14)	1.802(9)	2.644(17)	165.55(10)
C40-H40…O19	0.927(20)	2.328(7)	3.19(2)	154.55(11)

Table III.5. CH...π interactions in **4**.

CH...π	H...π (Å)
C40-H40...π {N3N4}	3.057(1)
C21-H21...π {N9N10}	3.258(1)
C16-H16...π {N7N8}	2.973(1)
C19-H19...π {N7N8}	3.278(1)

III.3.3. Crystal structure of 5 and 6

5 and **6a** are new supramolecular isomers of previously reported hybrid solid {4-H*ap*}$_6$[$P_2Mo_5O_{23}$].5H_2O, **6b** [15]. BVS calculations indicated that both the phosphate groups per cluster anion of **5** were protonated. On the other hand in **6a**, only one of the phosphate groups of cluster anion was protonated and in **6b**, the phosphate groups are not protonated. Interestingly, the topology of {4-H*ap*}$^+$ moieties, the cluster anion and lattice water molecules varies significantly in the three supramolecular isomers. While asymmetric unit of **5** consists of one {$H_2P_2Mo_5$} cluster anion, four monoprotonated {4-H*ap*}$^+$ moieties and two lattice water molecules; **6a** showed the presence of one {HP_2Mo_5} cluster anion and five {4-H*ap*}$^+$ moieties per asymmetric unit (refer Figure III.6).

The crystal structure analysis of **5** suggested that of the four {4-H*ap*}$^+$ moieties, {N1N2} and {N5N6} moieties linked {$H_2P_2Mo_5$} cluster anions to form 2-D sheet through N-H…O interactions (2.069(3)-2.208(3) Å) as shown in Figure III.7 (also refer Table III.6). The 2-D sheet showed the presence of voids which were occupied by the third {4-H*ap*}$^+$ moieties *viz.* {N7N8}. Each 2-D sheet was connected to two other sheets to form a 3-D supramolecular assembly (refer Figure III.8a) through {N1N2} and lattice water molecule, O1W via C-H…O (2.287(4) Å) and O…O interactions (refer Table III.7) respectively. The crystal packing of 2-D sheets further resulted in voids which were occupied by the fourth {4-H*ap*}$^+$ moiety *viz.* {N3N4} along with lattice water molecule, O2W. The occurrence {N3N4} moiety in the voids between 2-D sheets is also assisted by CH…π interactions between {N5N6}, {N3N4} and {N1N2} moieties as shown in Figure III.8b.

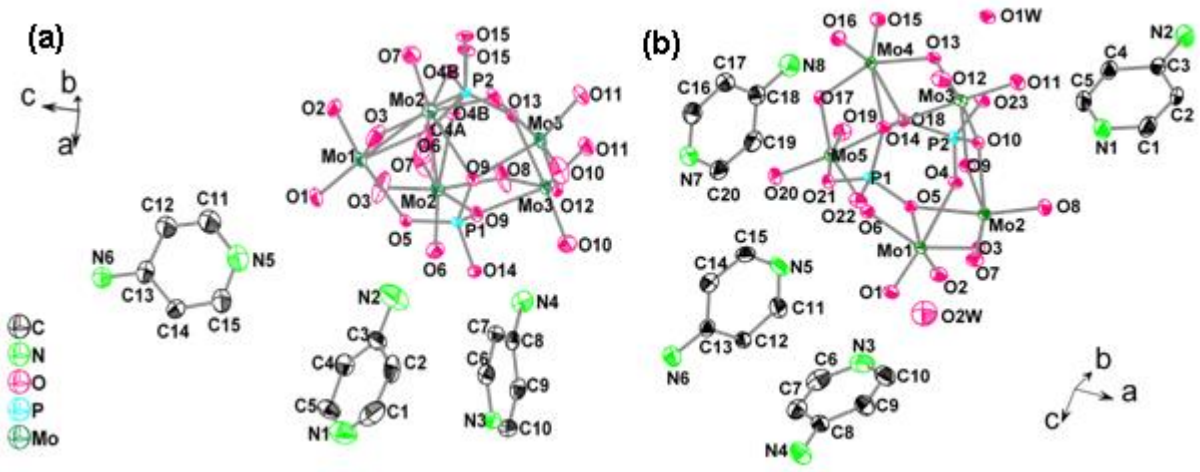

Figure III.6. ORTEP view of (a) **5** and (b) **6a**. The hydrogen atoms have been omitted for clarity.

Table III.6. H-bonding interactions in **5**.

D–H…A	D–H (Å)	H…A (Å)	D…A (Å)	∠ D–H…A (°)
N1-H1...O8	0.859(6)	2.087(4)	2.917(7)	162.32(34)
C1-H1A…O7	0.930(5)	2.287(4)	3.055(8)	139.57(35)
N2-H2A…O4	0.859(6)	2.208(3)	3.014(7)	156.03(41)
N3-H3…O2W	0.860(6)	2.045(7)	2.877(10)	162.46(39)
N4-H4A…O11	0.860(5)	2.377(2)	3.003(5)	130.07(31)
N5-H5…O21	0.860(5)	2.069(3)	2.812(5)	144.24(27)
N6-H6B…O17	0.860(4)	2.208(3)	3.047(5)	165.30(29)
N7-H7…O12	0.860(6)	2.346(5)	2.973(8)	130.03(32)
N8-H8Y2…O16	0.859(6)	2.286(4)	2.955(8)	134.88(39)

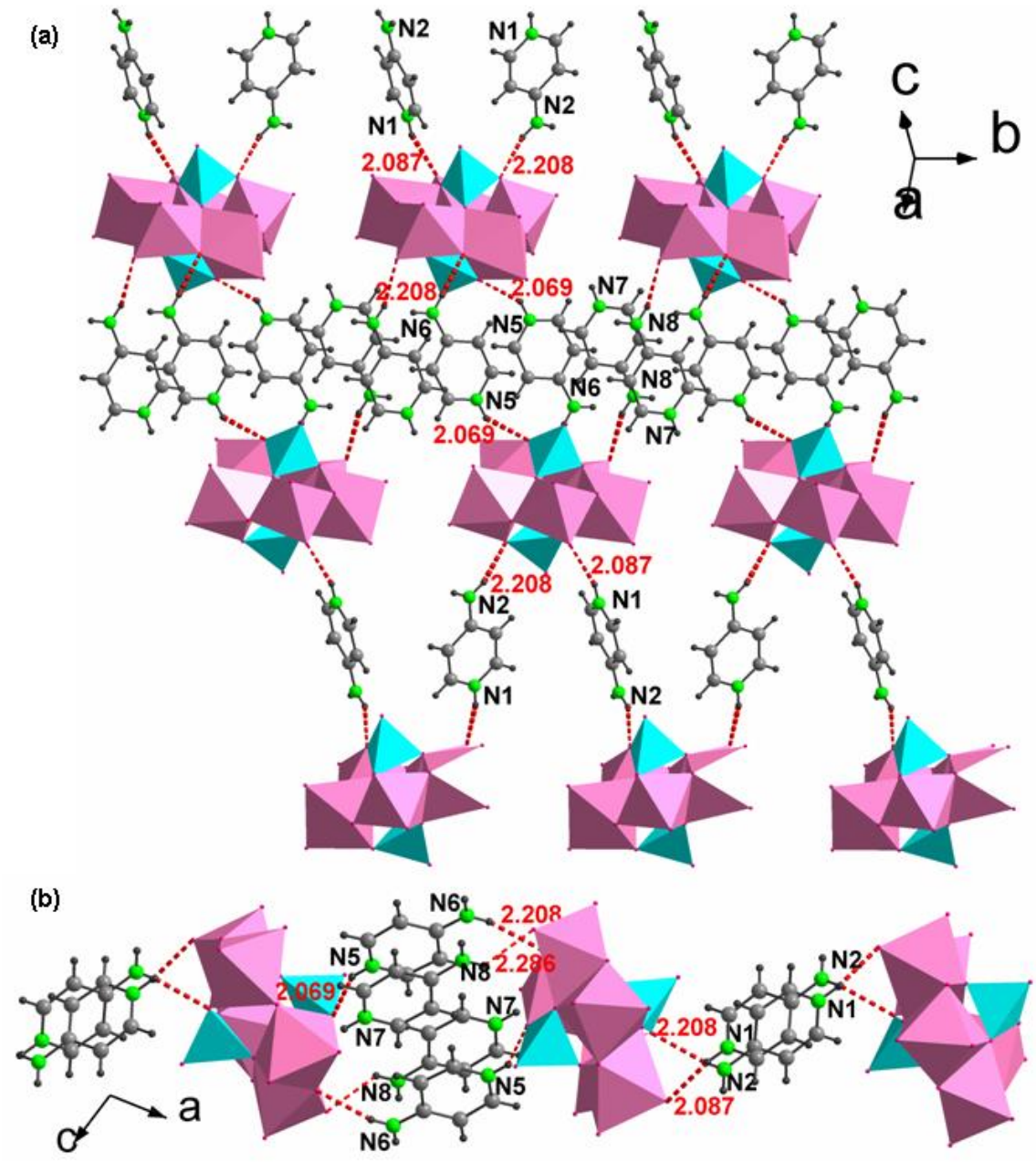

Figure III.7. (a) NH…O interactions mediated by {N1N2} and {N5N6} moiety link {$H_2P_2Mo_5$} cluster anions to form 2-D sheet through N-H…O interactions (2.069(3)-2.208(3) Å). The third (H*ampy*)$^+$ moiety *viz.* {N7N8} is encapsulated in the voids of 2-D sheet through N-H…O interaction (2.286(4) Å). (b) View along *b* axis.

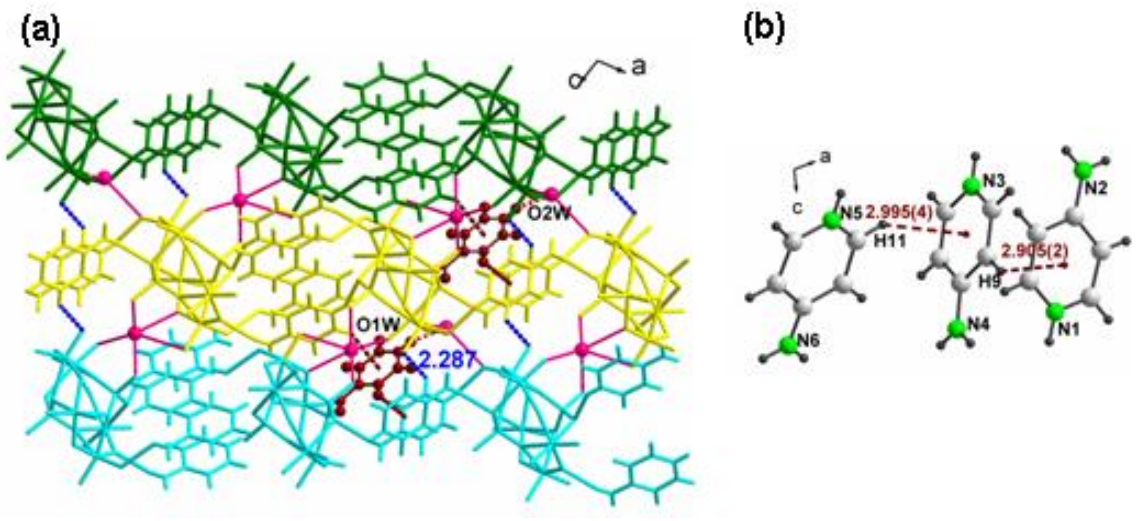

Figure III.8. (a) Figure showing packing of sheets. Three such sheets are shown in green, yellow and cyan. Two of the sheets are connected via H-bonding interactions mediated by {N1N2} and lattice water molecule, O1W. The inter-sheet H-bonding and O…O interactions are depicted in dashed blue and solid red color respectively. The voids formed as a result of crystal packing of 2-D sheets are occupied by {N3N4} moieties and lattice water molecule, O2W shown in brown and pink color respectively. (b) CH…π interactions between {N5N6}, {N3N4} and {N1N2} are shown in dashed brown lines.

Table III.7. O...O interactions in **5**.

Sl. No.	O…O	Distance (Å)
1	O1W…O1	2.767(5)
2	O1W…O13	2.655(6)
3	O1W…O22	2.719(7)
4	O1W…O23	2.622(5)
5	O2W…O8	2.933(7)
6	O2W…O2	2.902(5)

On the other hand, in **6a**, through H-bonding interactions mediated by {N3N4}, {4-H*ap*}$^+$ moieties and {P_2Mo_5} cluster anions form 1-D zig-zag chains. The 1-D chains propagate

along *b*-axis. The 1-D chains are connected through H-bonding interactions mediated by {N5N6} moieties to form 2-D corrugated sheet having voids which are occupied by {N1N2} moieties. CH…π and π…π interactions between {N1N2}…{N3N4} and {N3N4}…{N3N4} moieties respectively favor the incorporation of {N1N2} units in the voids of the 2-D corrugated sheets. CH…π and π…π interactions between {N1N2} and {N3N4} moieties form a tetrameric unit which is incorporated within the 2-D corrugated sheet (refer Figure III.9, III.10 and III.11). Further {N1N2} moieties link neighboring 2-D corrugated sheets via H-bonding interactions (shown in dashed red lines) to form a supramolecular 3-D framework. CH…π interactions between the tetrameric units and {N5N6} moieties of neighboring 2-D corrugated sheets form 1-D zig-zag chains which further reinforces the supramolecular crystal packing in **6a**.

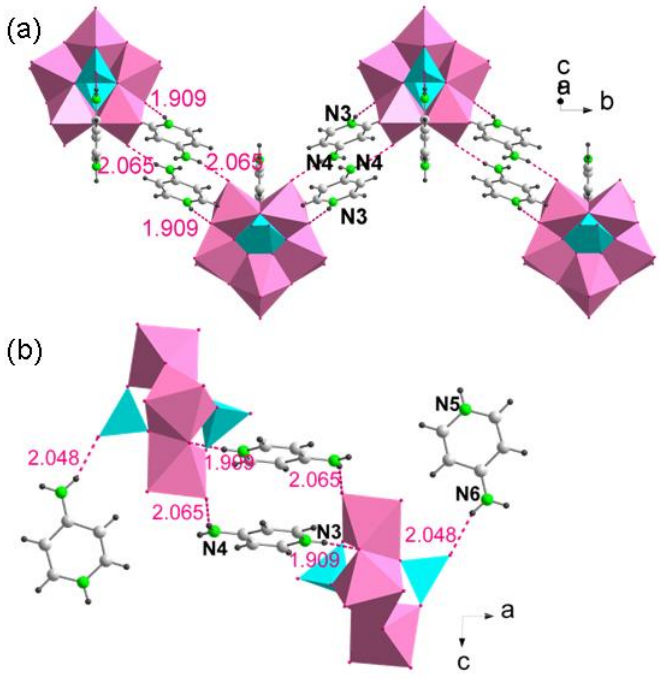

Figure III.9. (a) H-bonding interactions (shown in dashed red lines) between {4-H*ap*}$^+$ moieties and {P_2Mo_5} cluster anions forming 1-D zig-zag chains in **6a**. (b) View along *b*-axis.

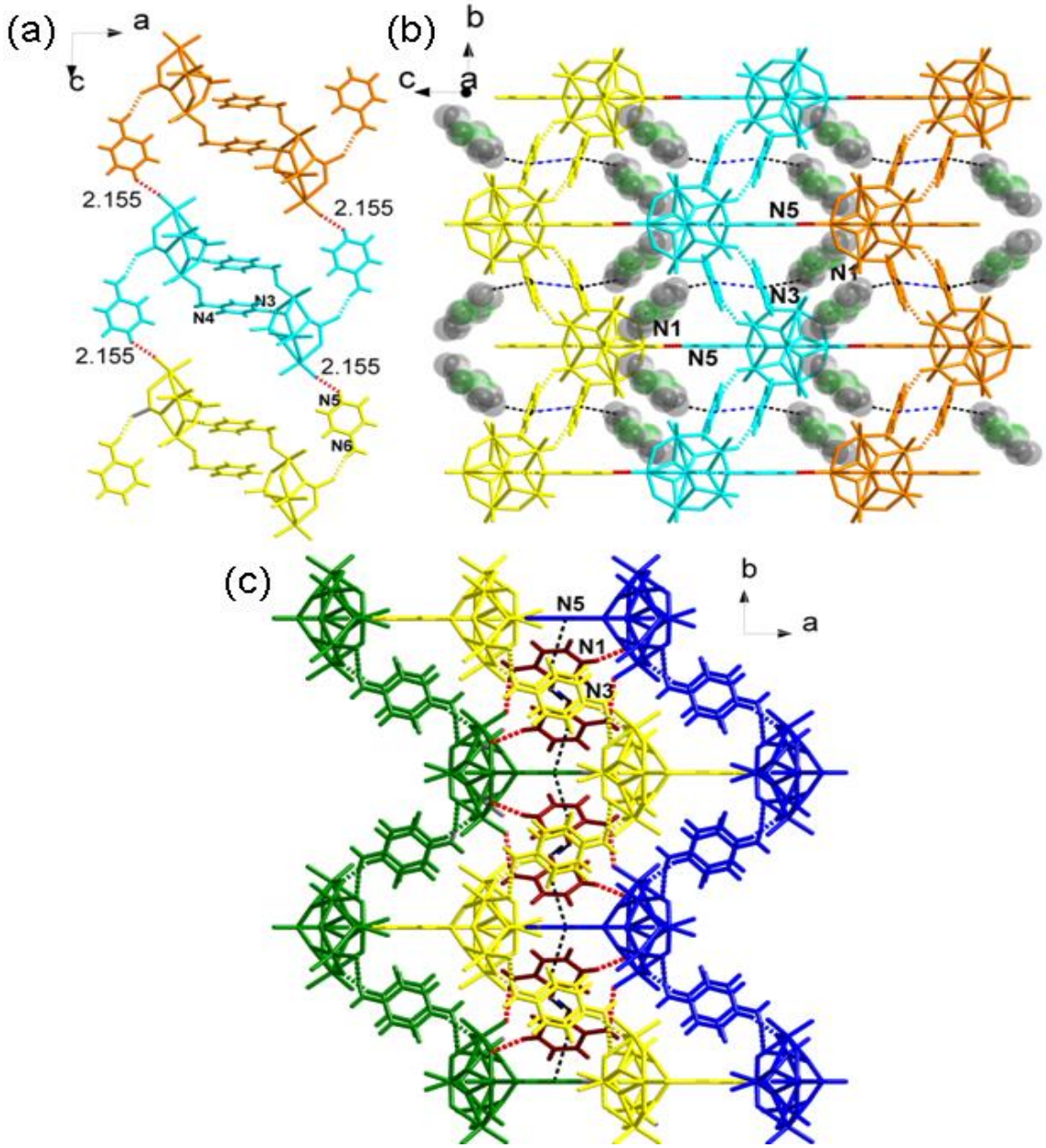

Figure III.10. (a) The 1-D chains are connected through H-bonding interactions mediated by {N5N6} moieties to form 2-D corrugated sheet having voids. Three such chains are shown in orange, cyan and yellow color. (b) Figure showing 2-D corrugated sheet having voids are occupied by {N1N2} moieties CH…π and π…π interactions between {N1N2} and {N3N4} moieties form a tetrameric unit. The interactions are shown in dashed black and blue color respectively. (c) Three of the 2-D corrugated sheets are shown in green, yellow

and blue. Each sheet exhibits H-bonding interactions with neighboring sheets through {N1N2} moieties (shown in brown color) accommodated in its voids. The tetramers are connected through CH…π interactions mediated by {N5N6} moieties belonging to neighboring 2-D corrugated sheets.

Table III.8. H-bonding interactions in **6a**.

D–H…A	D–H (Å)	H…A (Å)	D…A (Å)	∠ D–H…A (°)
N1-H1...O3	0.860(13)	2.201(22)	3.032(31)	162.50(75)
N2-H2B…O6	0.859(12)	2.194(6)	2.984(14)	152.94(79)
N3-H3…O8	0.860(7)	1.909(9)	2.722(13)	157.11(46)
N4-H4A…O11	0.861(8)	2.065(5)	2.886(10)	159.26(53)
N5-H5…O1	0.860(16)	2.155(32)	2.867(47)	139.84(97)
N6-H6B…O14	0.860(16)	2.048(25)	2.874(40)	160.47(72)
C1-H1A…O7	0.930(16)	2.381(12)	3.283(23)	163.45(85)
C5-H5A…O5	0.930(12)	2.385(19)	3.204(30)	146.69(61)
C6-H6…O15	0.929(8)	2.331(10)	3.243(14)	166.95(52)
C10-H10…O10	0.929(10)	2.426(31)	3.254(38)	148.46(53)
C12-H12…O12	0.931(20)	2.263(32)	3.190(48)	173.83(89)

Table III.9. CH…π and π…π interactions in **6a**.

CH…π	CH…π (Å)	π…π	π…π (Å)
C2-H2...π{N3N4}	2.837(18)	π{N3N4}… π{N3N4}	3.610(5)
C9-H9...π{N5N6}	3.244(9)		

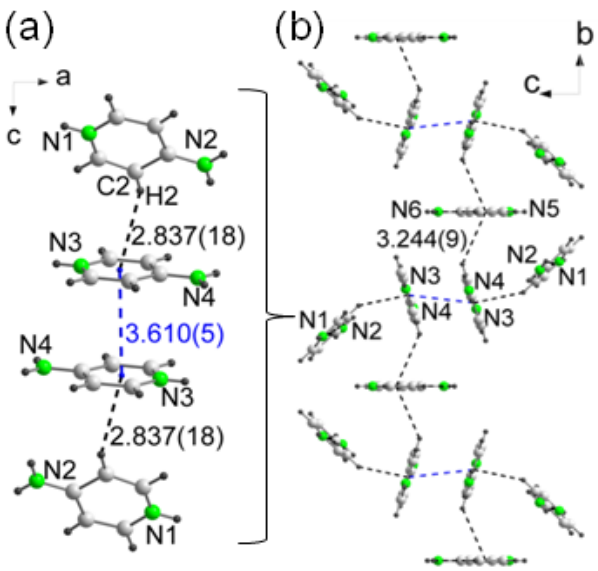

Figure III.11. (a) CH…π and π…π interactions between {N1N2} and {N3N4} moieties form a tetrameric unit. The interactions are shown in dashed black and blue color respectively. (b) The tetramers are connected through CH…π interactions mediated by {N5N6} moieties.

In {4-H*ap*}$_6$[$P_2Mo_5O_{23}$].5H_2O, **6b** {P_2Mo_5} cluster anions are linked by {N3N4} moieties to form a dimeric unit, which are further connected via {N11N12} moieties (N12H12B…O11: 2.018(8) Å) to form 1-D chains. {N1N2}, {N7N8} and {N9N10} units remain anchored to the dimeric units through NH…O interactions as shown in Figure III.12 (also refer Table III.10 for H-bonding interactions in **6b**). The 1-D chains are connected through H-bonding interactions mediated by {N9N10} moiety to form 2-D sheet. The formation of sheet resulted in inter-chain voids which are occupied by {N3N4} moieties (refer Figure III.13). These moieties act as templates through which 2-D sheets are formed along with lattice water molecules. It is interesting to note the interpenetrating nature of 2-D sheets in **6b** (Figure III.14).

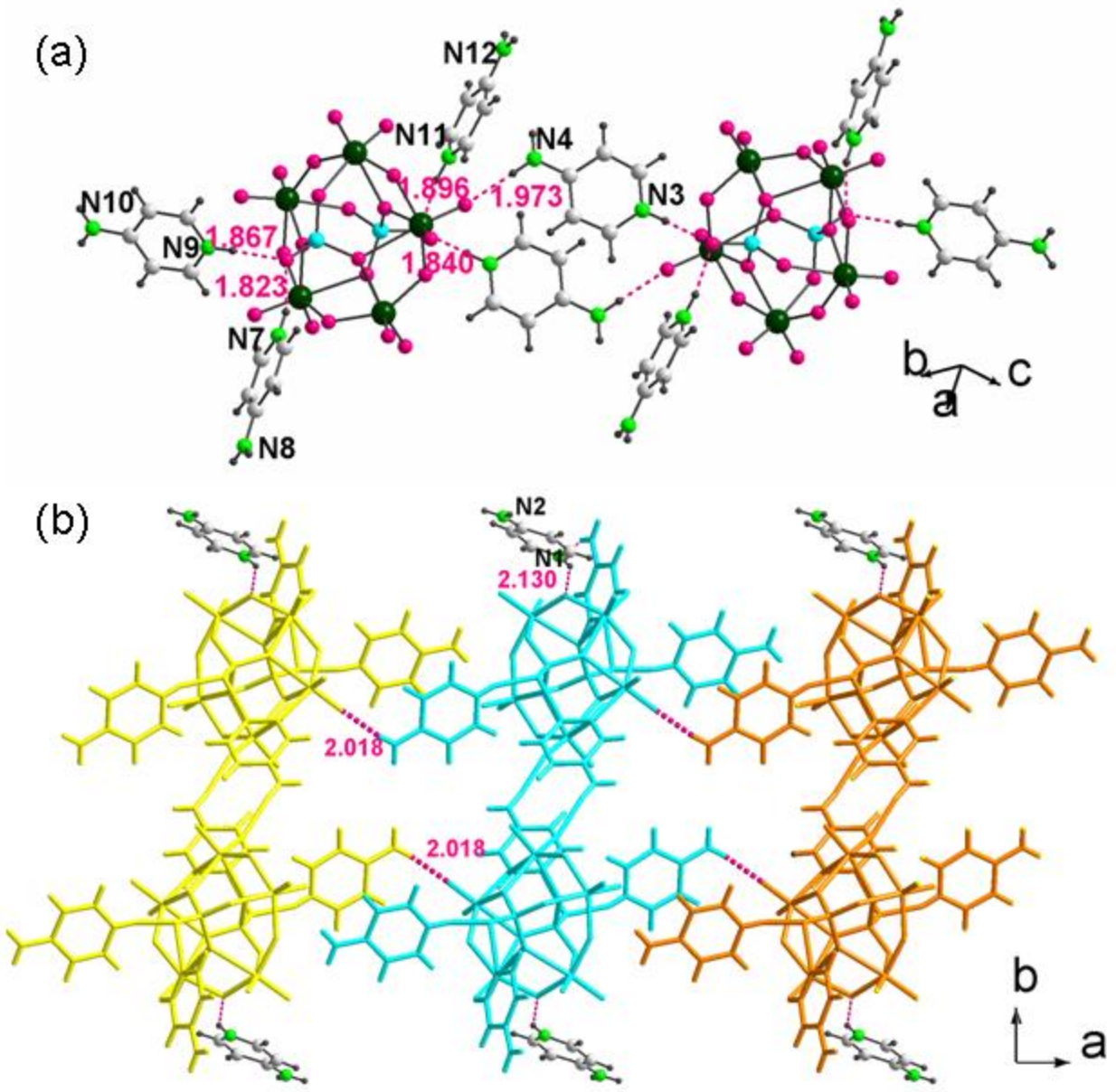

Figure III.12. (a) Figure showing the formation of dimeric unit in **6b**. (b) Each of the dimeric units (three such dimeric units are shown in yellow, cyan and orange) is connected via H-bonding interactions to form 1-D chains.

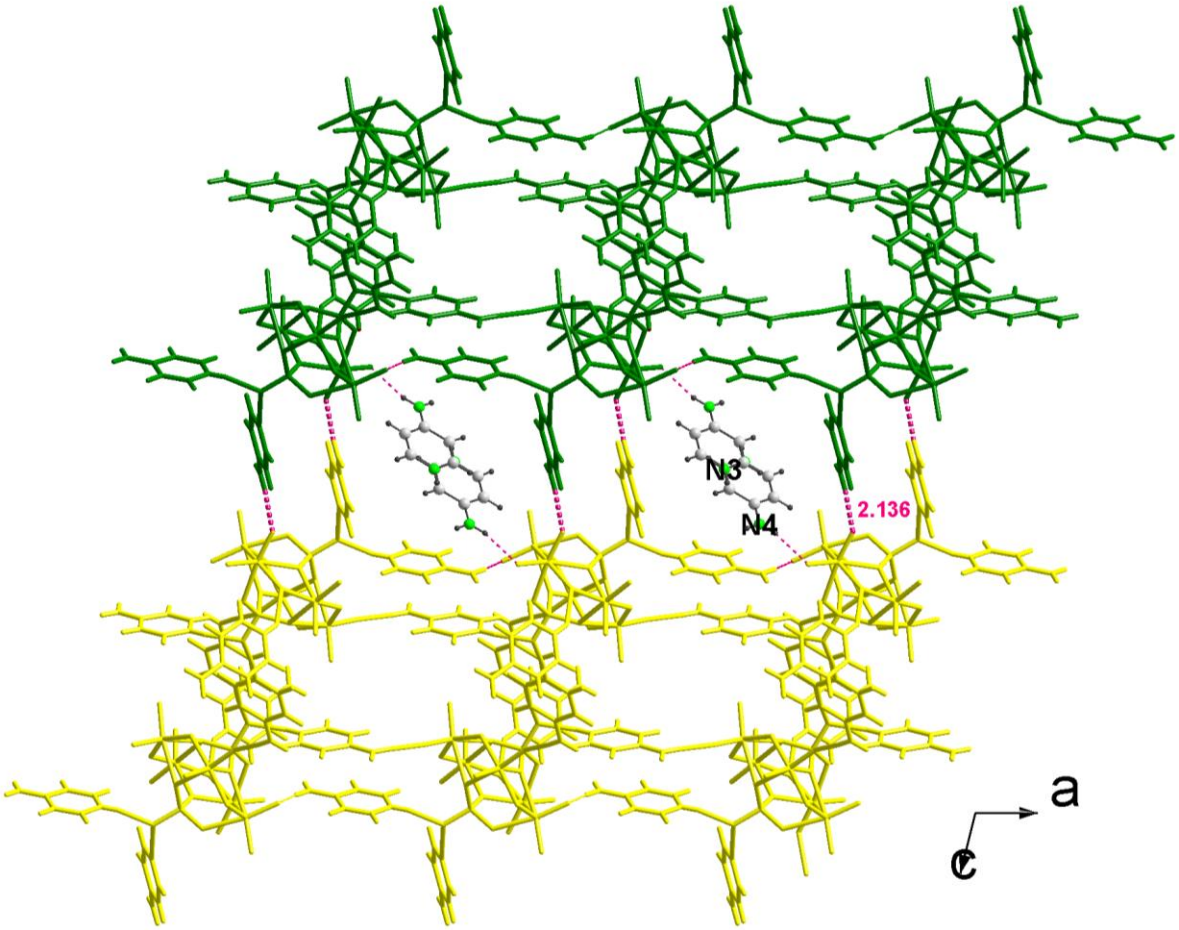

Figure III.13. Figure showing two 1-D chains (depicted in yellow and green color) connected via H-bonding mediated by {N9N10} moieties (2.136 (25) Å). The inter-chain voids are occupied by {N3N4} units.

Table III.10. H-bonding interactions in **6b**.

D–H…A	D–H (Å)	H…A (Å)	D…A (Å)	∠ D–H…A (°)
N1-H1...O15	0.859(18)	2.316(12)	3.010(16)	138.12(99)
N1-H1…O17	0.859(18)	2.130(7)	2.847(17)	140.84(95)
N2-H2A…O2	0.861(14)	2.248(38)	3.054(51)	155.95(63)
N2-H2B…O14	0.862(12)	2.210(14)	3.060(24)	169.09(56)
N3-H3…O23	0.861(11)	1.840(15)	2.692(23)	170.11(60)

N4-H4A…O7	0.86(1)	1.973(7)	2.822(13)	168.69(62)
N4-H4B…O19	0.860(15)	2.159(40)	3.003(54)	166.78(59)
N5-H5A…O5W	0.859(15)	2.006(22)	2.851(35)	167.88(63)
N6-H6A…O3	0.861(15)	2.305(19)	3.073(25)	148.55(93)
N6-H6B…O16	0.859(16)	2.312(36)	3.159(48)	168.69(88)
C15-H15…O3W	0.93(1)	2.365(11)	3.288(15)	171.38(59)
N7-H7…O22	0.86(1)	1.823(22)	2.660(28)	163.86(60)
N8-H8B…O1	0.859(9)	2.180(7)	2.996(13)	158.50(58)
N9-H9…O22	0.860(8)	1.867(7)	2.724(11)	174.93(54)
N10-H10B…O20	0.861(16)	2.136(25)	2.971(39)	163.26(71)
C25-H25…O16	0.929(17)	2.312(7)	3.150(18)	149.88(66)
N11-H11…O23	0.859(9)	1.896(10)	2.720(17)	160.14(58)
N12-H12B…O11	0.86(1)	2.018(8)	2.871(14)	171.37(61)
C26-H26…O7	0.930(11)	2.459(7)	3.386(14)	174.54(64)
C27-H27…O19	0.930(11)	2.369(6)	3.294(13)	172.61(69)

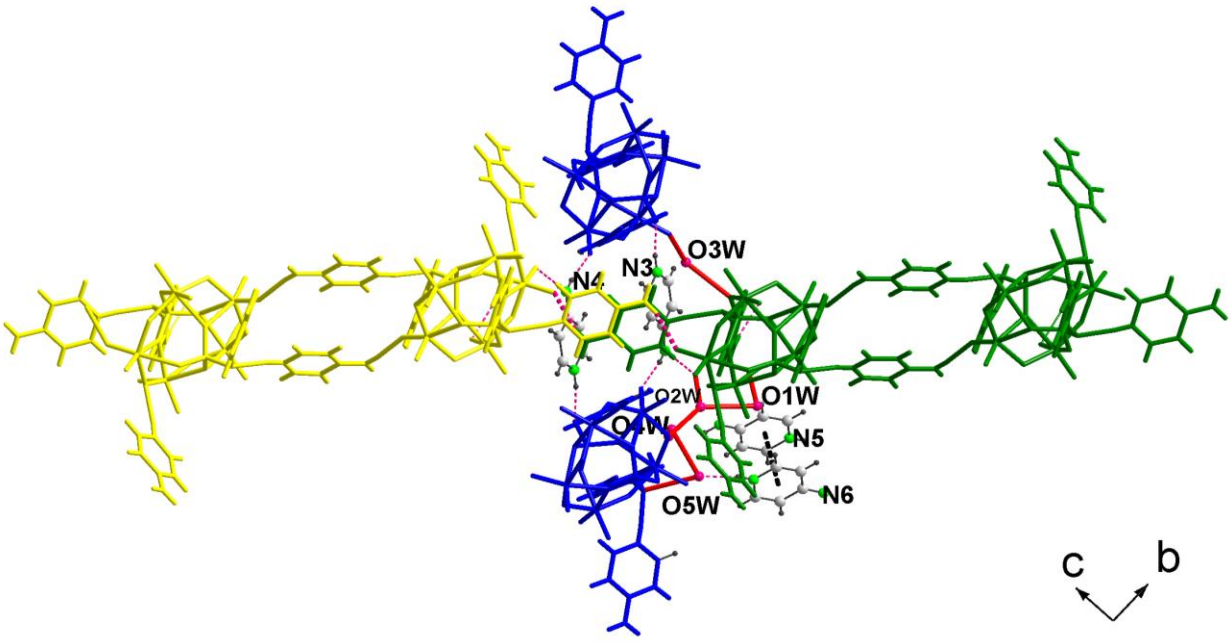

(a)

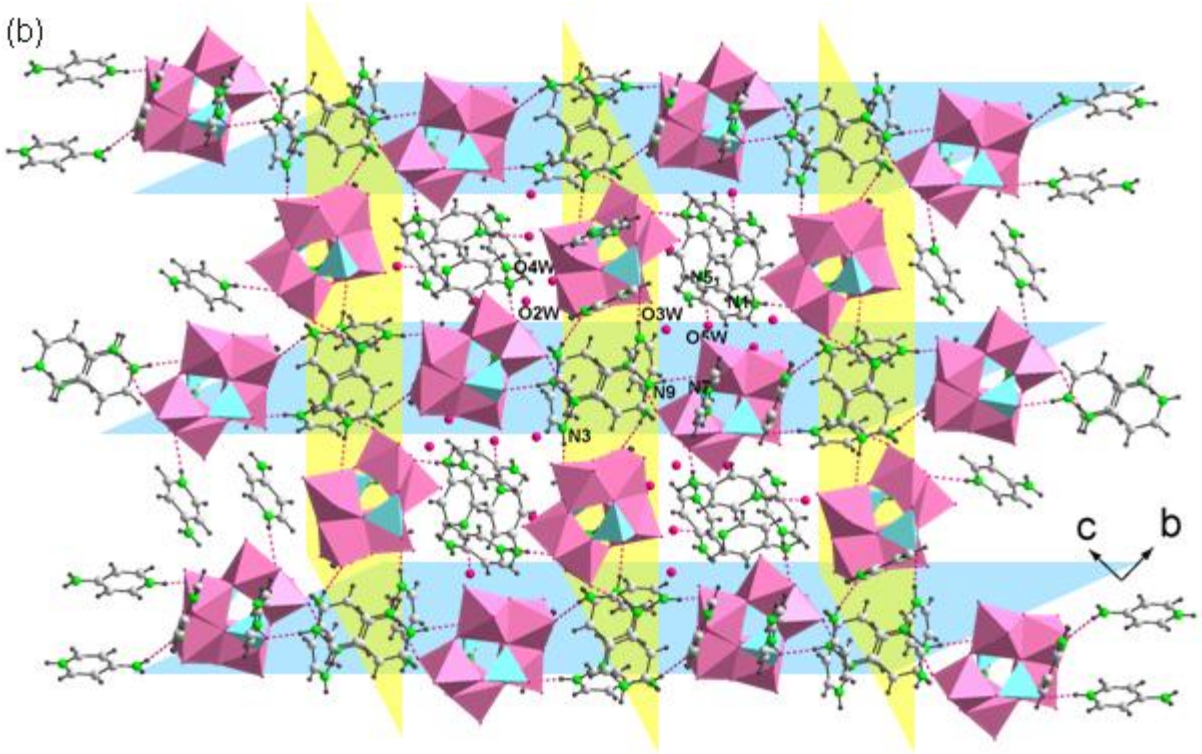

Figure III.14. (a) The {N3N4} units in inter-chain voids are part of interpenetrating 2-D sheets perpendicular to sheet shown in Figure III.13. The lattice water molecules along with {N3N4} units act as nodes connecting the interpenetrating sheets. Inter-sheet spaces are occupied by {N1N2} and {N5N6} moieties (π...π: 3.550 Å) which are anchored to lattice water molecule O5W. (b) Figure showing the two sets of interpenetrating sheets.

III.3.4. Analysis of solids 3-6

FTIR spectra (Figure III.15 and 16) exhibited bands characteristic of P–O and Mo–O stretching which indicated the presence of PMO cluster anion in Solids **3-6a**. The bands corresponding to organic moieties in **3-6a** were also found to be in good agreement with C-H, N-H, C-N and O-H stretching frequency with those reported in literature [18].

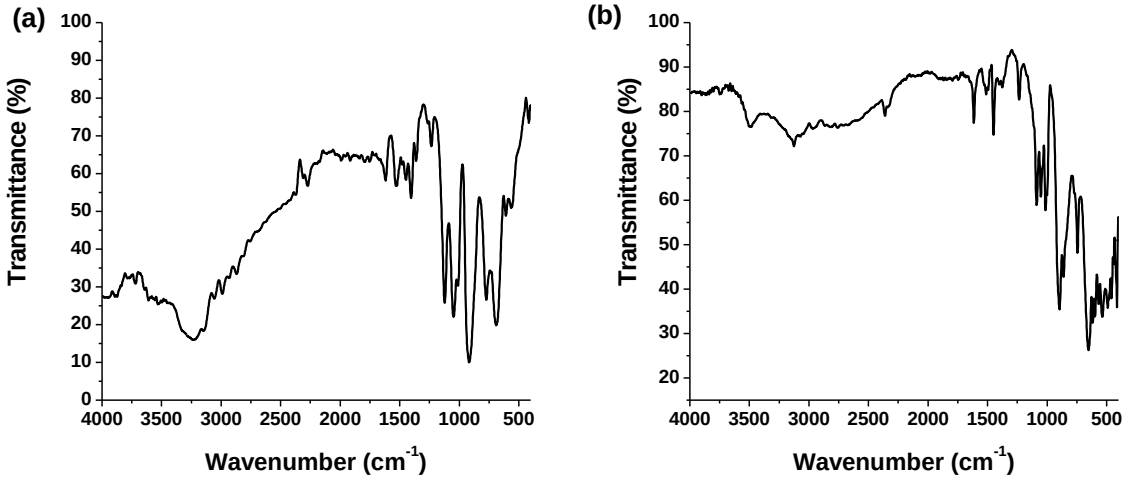

Figure III.15. FTIR spectrum of (a) **3** and (b) **4**.

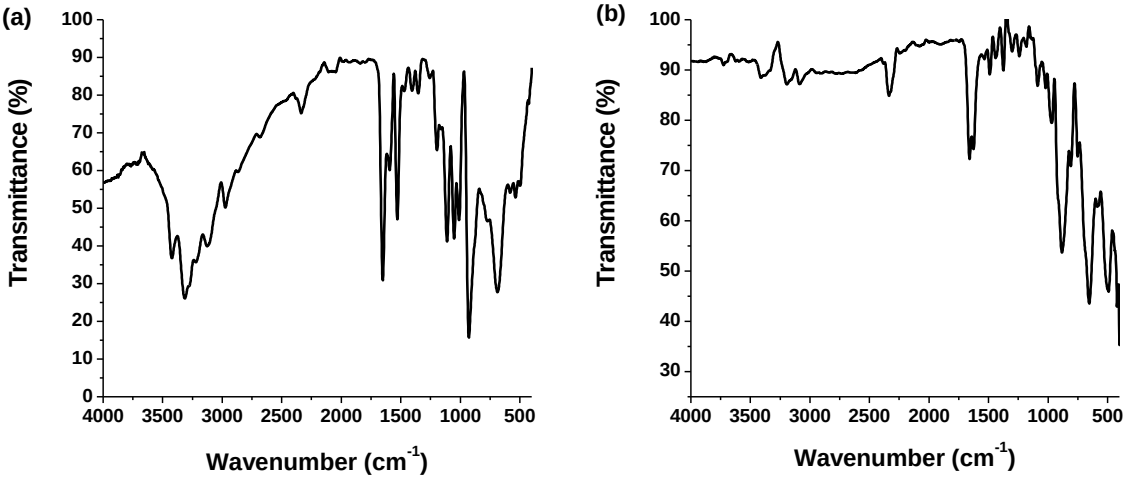

Figure III.16. FTIR spectrum of (a) **5** and (b) **6a**.

In solids **3-6**, the phase purity of the solids was established by comparing the experimental PXRD pattern with simulated powder pattern of the single crystal structure as shown in Figures III.17-21.

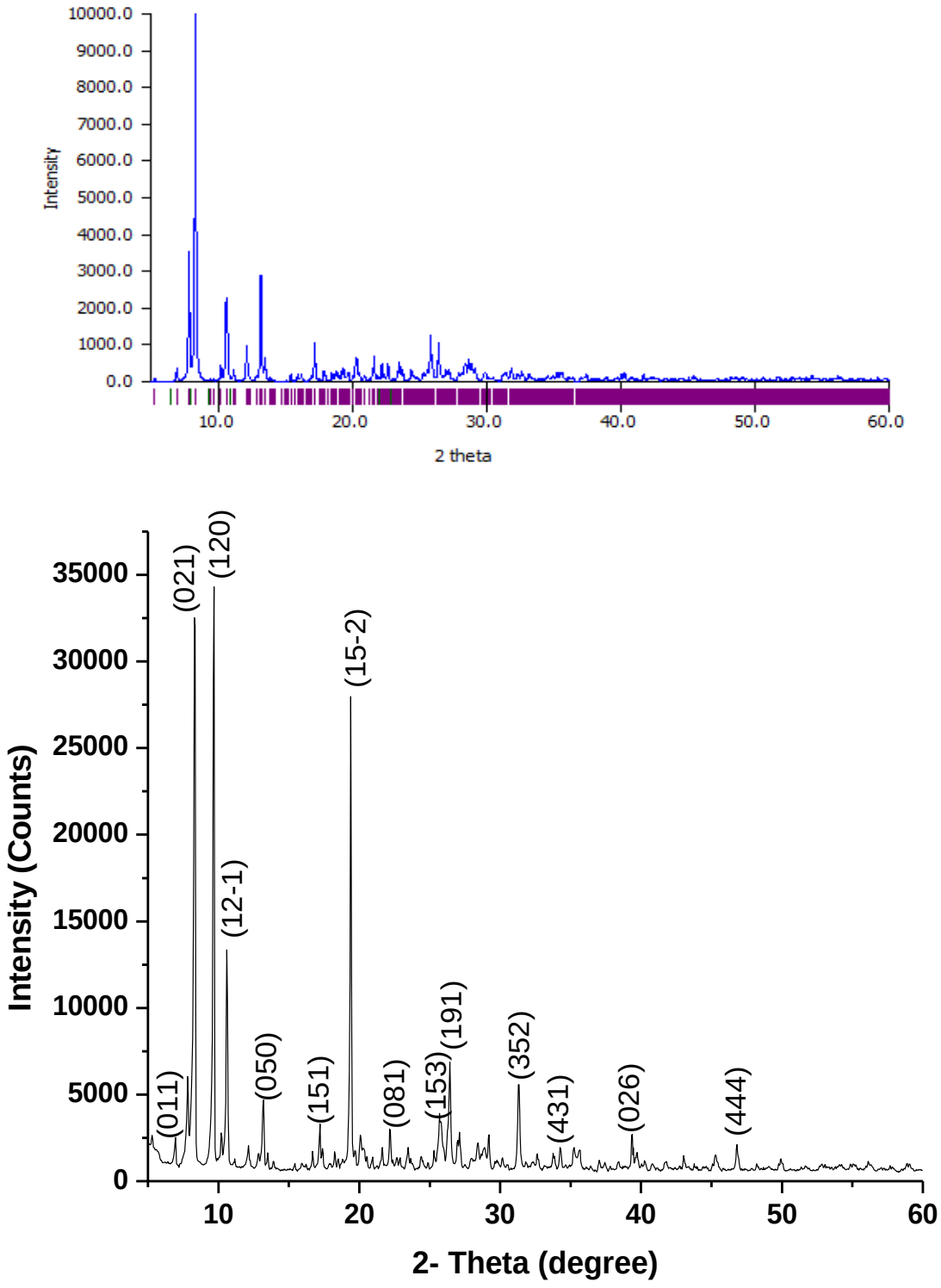

Figure III.17. Simulated (top) and Experimental (bottom) PXRD of **3**.

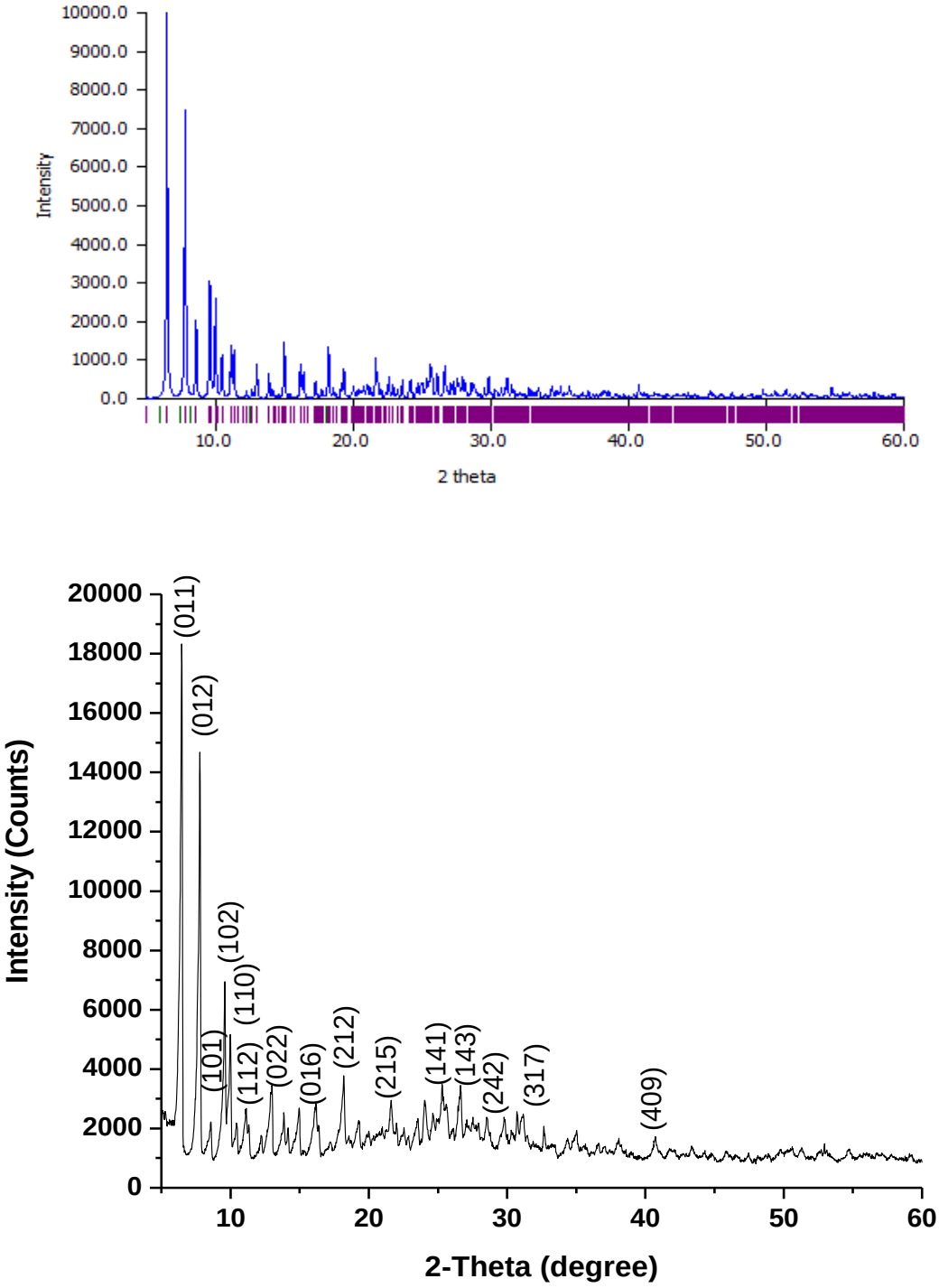

Figure III.18. Simulated (top) and Experimental (bottom) PXRD of **4**.

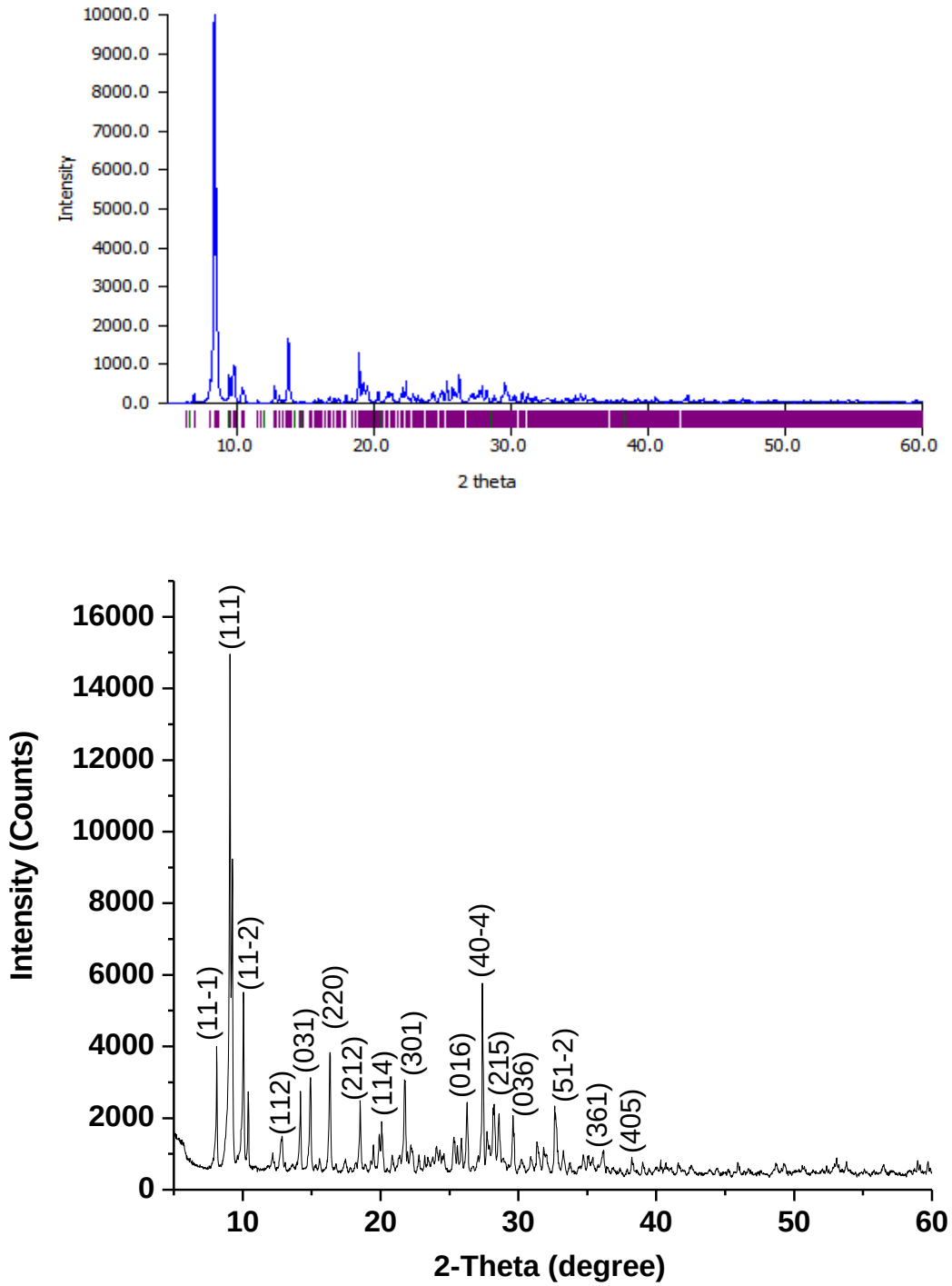

Figure III.19. Simulated (top) and Experimental (bottom) PXRD of **5**.

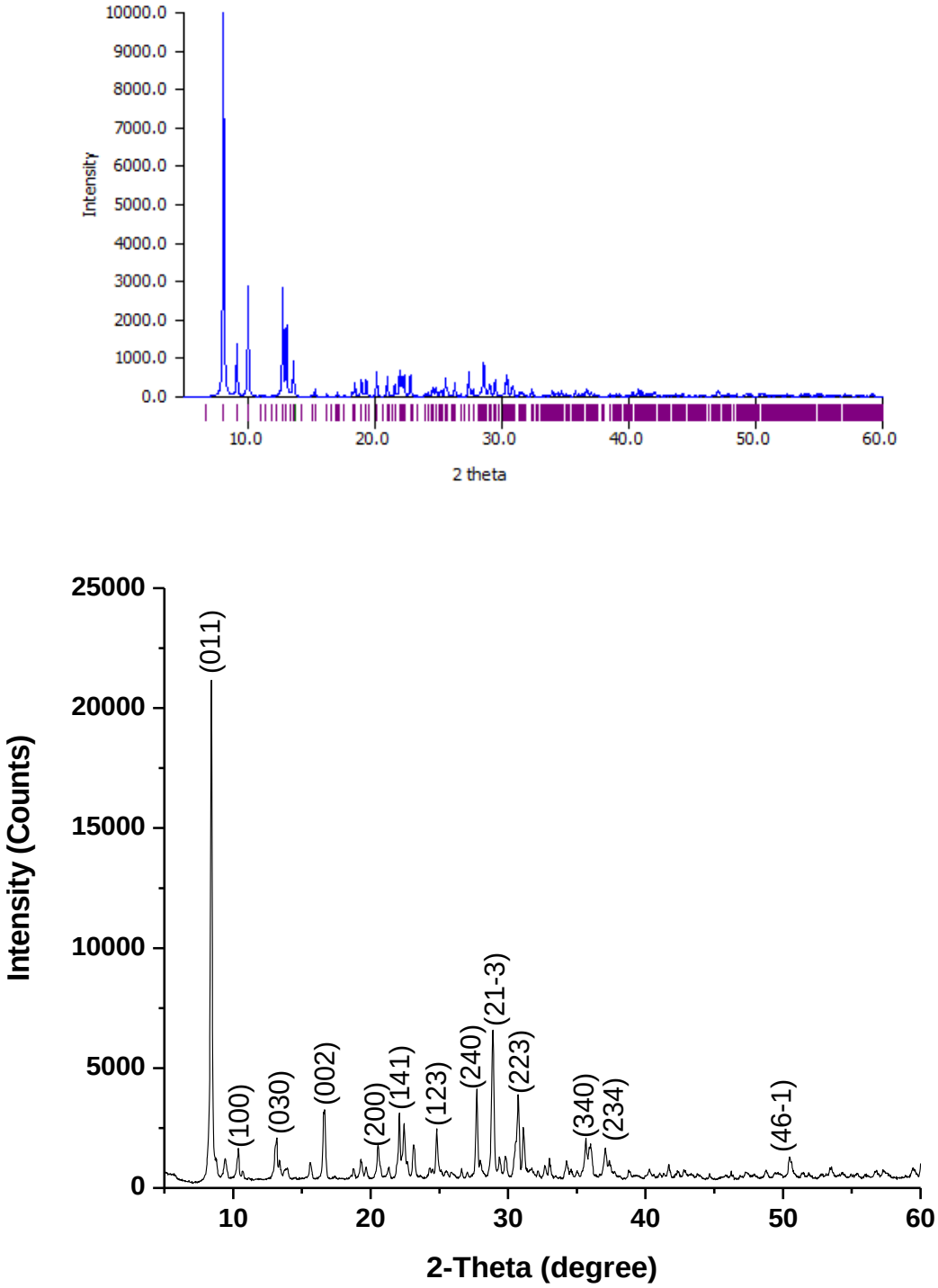

Figure III.20. Simulated (top) and Experimental (bottom) PXRD of **6a**.

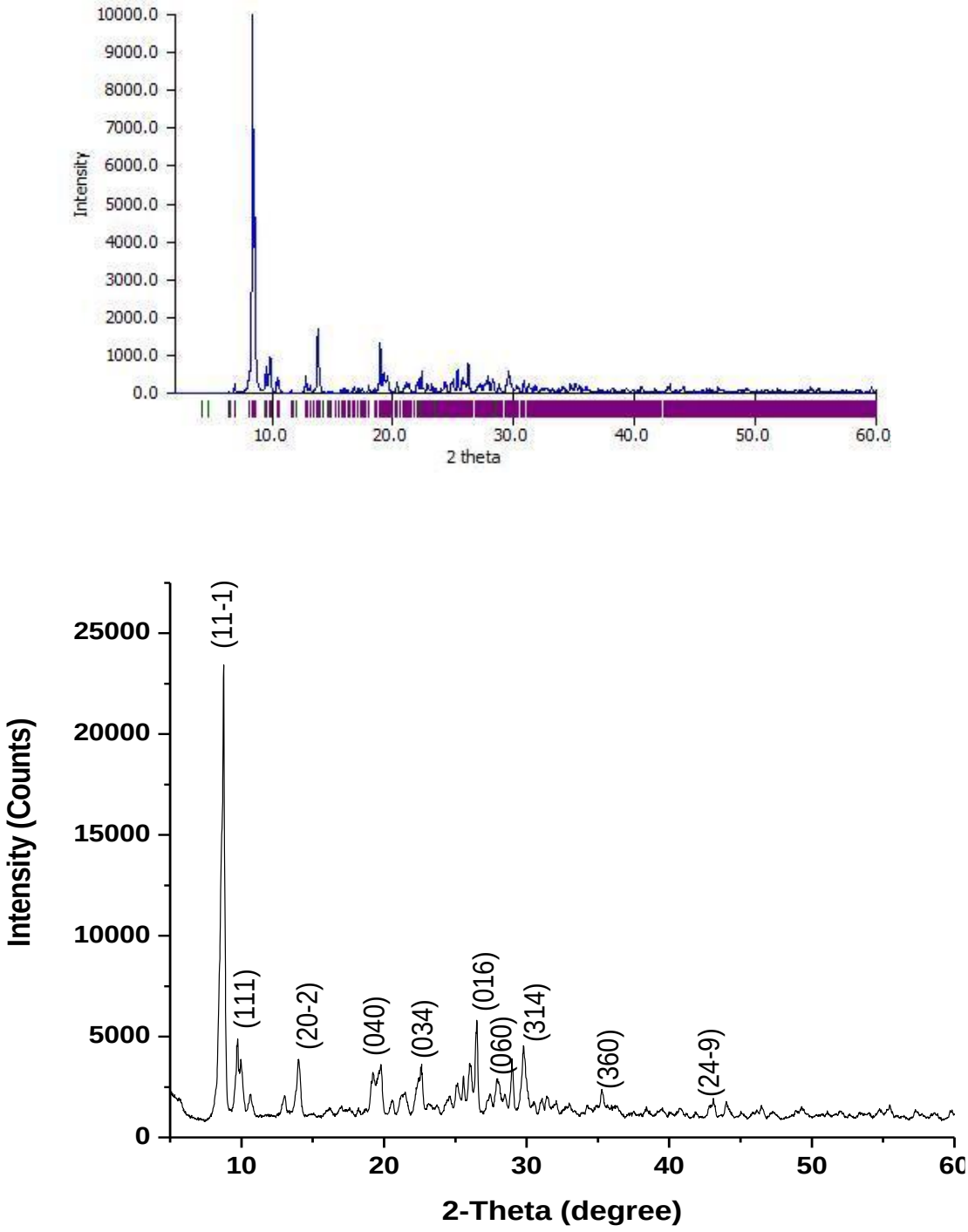

Figure III.21. Simulated (top) and Experimental (bottom) PXRD of **6b**.

Thermo gravimetric analysis (TGA) of only solids **4**, **5** and **6a** was carried out (refer Figure III.22) as TGA of **3** and **6b** has already been reported in literature. The TGA of **4** showed weight loss in two steps. The first weight loss corresponding to ~35% could be attributed to the thermal degradation of water molecule and five protonated benzimidazole moieties (theoretical value: 37.19%). The second step was attributed to the decomposition of {P_2Mo_5} cluster anion. In **5**, the first weight loss (~ 2%) at 120^{o}C was attributed to the loss of two water molecules (theoretical value: 2.71%). The weight loss of ~19% (theoretical value: 21.4%) in the second step was attributed to the degradation of three protonated 4-*ap* moieties, followed by decomposition of {P_2Mo_5} cluster anion. The ~20% weight loss observed in **6a** below 400^{o}C was assigned to the degradation of three protonated 4-*ap* moieties (theoretical value: 20.5%). The second weight loss upto 800^{o}C attributed to the loss of the remaining two organic ligands and decomposition of {P_2Mo_5} cluster anion.

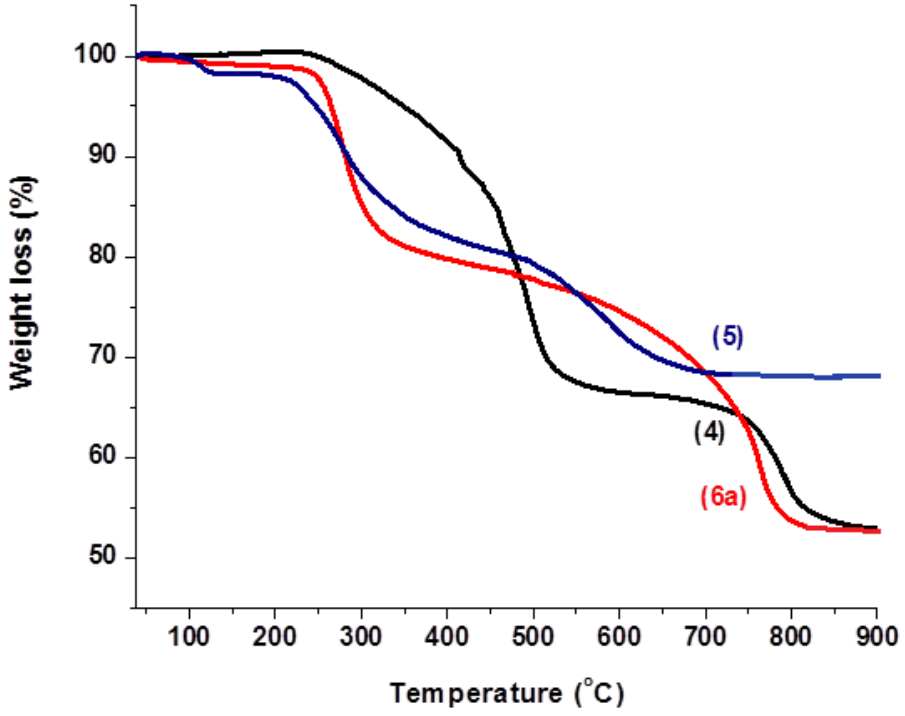

Figure III.22. TGA of **4**, **5** and **6a**.

III.3.5. Band gap energy calculations

The band gap enrgy was determined using Kubelk- a–Munk (KeM or F(R)) function in Tauc method. The method was discussed in Chapter II, section II.3.4.

III.3.5.1. Effect of ligands on band gap energy

In order to study the effect of ligands, the optical band gap energy was calculated from the DRS data for solids **3** and **6a** which are based on {HP_2Mo_5} clusters (refer Figure III.23 and III.24) were also compared with the E_g of monoprotonated solids **1** and **2** discussed in Chapter II (refer Table III.11). The E_g values showed slight variations on account of different ligands present in the solids and difference in the coordination atmosphere of the monoprotonated cluster anion. While, in all the four cases, allowed direct band gap energy showed low value; {H-2*a*4*mp*}$_5$[{PO_3(OH)}{PO_4}Mo_5O_{15}].6H_2O (**2**) and {H*bimi*}$_5$[$HP_2Mo_5O_{23}$].5H_2O (**3**) displayed the highest values for the irrespective, allowed indirect and allowed direct band gap energy which indicates that perphaps water of crystallization also plays some role in optical band gap energy. As discussed earlier, **2** and **3** have six and five molecules of water of crystallization associated with them respectively; however, **1** and **6a** are devoid of water of crystallization.

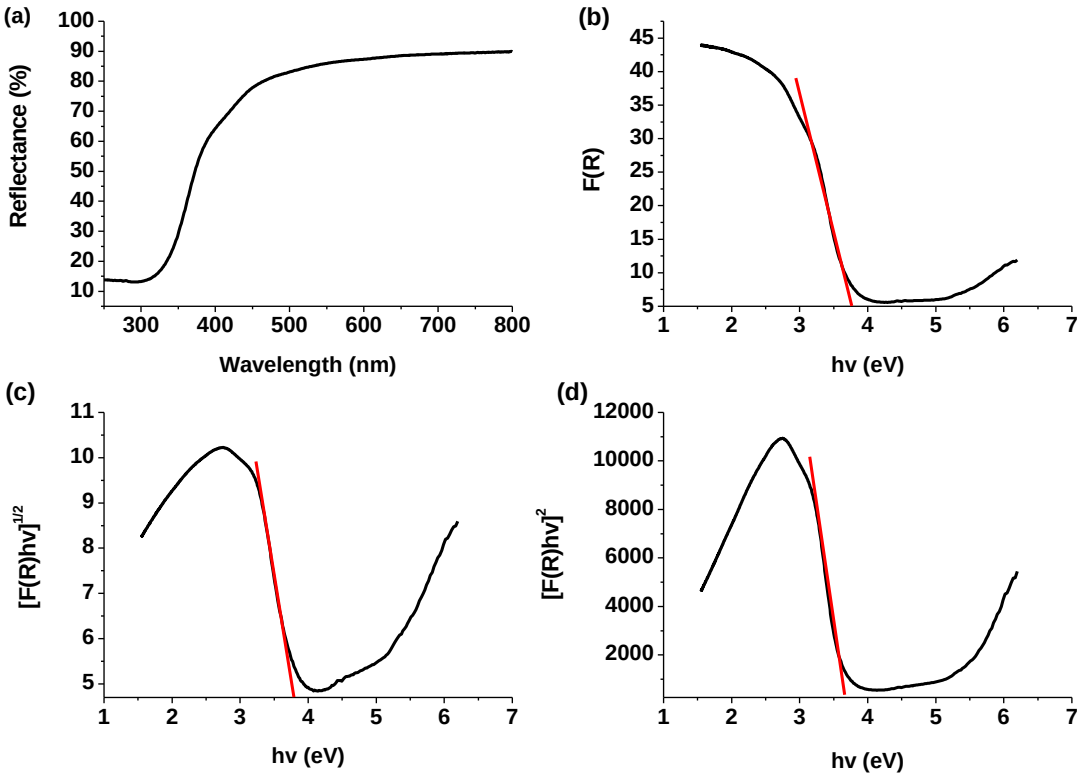

Figure III.23. Plots of (a) Reflectance versus wavelength (b) F(R) versus hυ(eV), (c) $(F(R)h\upsilon)^{1/2}$ versus hυ(eV) and (d) $(F(R)h\upsilon)^{2}$ versus hυ(eV) for **3**.

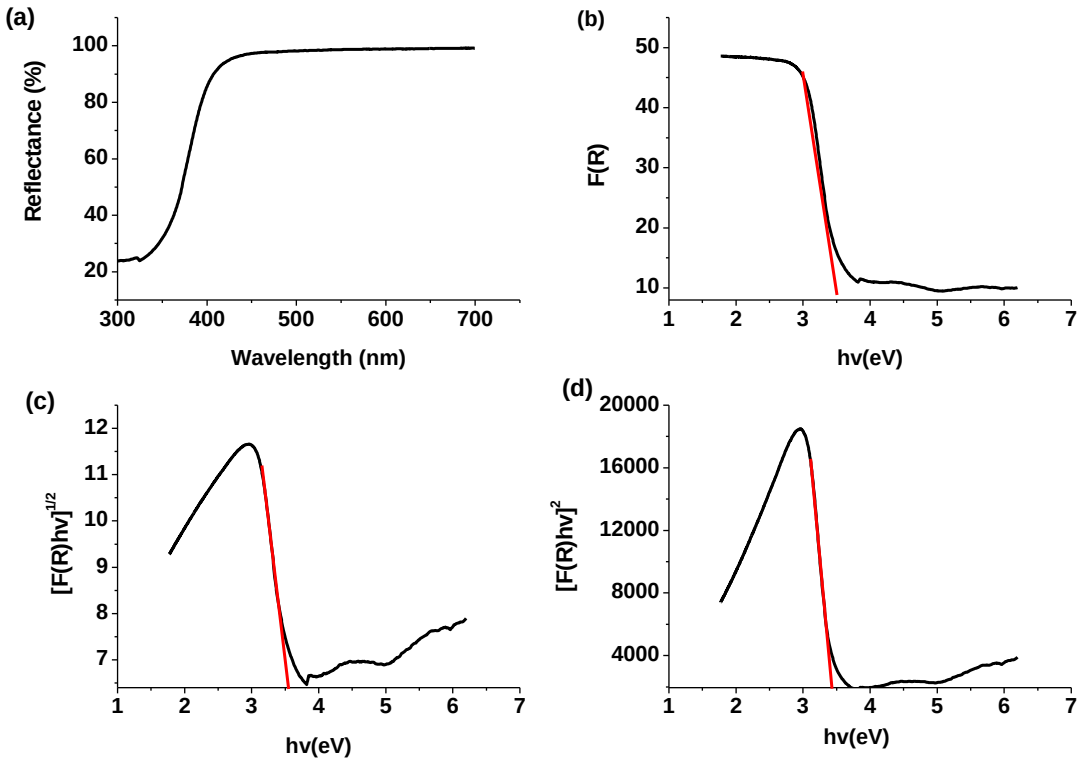

Figure III.24. Plots of (a) Reflectance versus wavelength (b) F(R) versus hυ(eV), (c) $(F(R)h\upsilon)^{1/2}$ versus hυ(eV) and (d) $(F(R)h\upsilon)^2$ versus hυ(eV) for **6a**.

Table III.11 Table tabulates the irrespective, allowed indirect and allowed direct band gaps of **1**, **2**, **3** and **6a**

Solids	F(R) vs hυ (band gap energy irrespective of direct or indirect in eV)	$[F(R)\ h\upsilon]^{1/2}$ (allowed indirect band gap energy in eV)	$[F(R)\ h\upsilon]^2$ (allowed direct band gap energy in eV)
1	3.67	3.66	3.53
2	3.75	3.81	3.55
3	3.75	3.78	3.63
6a	3.53	3.55	3.42

III.3.5.2. Effect of protonation on band gap energy

The optical band gap energy of **5**, **6a** and **6b** was calculated using DRS data to study the effect of protonation on E_g, since they are di-protonated, mono-protonated and unprotonated respectively (refer Figure III.24, 25, 26 and Table III.12). It is observed that the band gap energy decreased as the protonation increased. So, solid **6b** which has a non-protonated cluster centre showed highest band gap energy values.

Table III.12. Table tabulates the irrespective, allowed indirect and allowed direct band gaps of 5, **6a** and **6b**.

Solids	F(R) vs hυ (band gap energy irrespective of direct or indirect in eV)	$[F(R)\ h\upsilon]^{1/2}$ (allowed indirect band gap energy in eV)	$[F(R)\ h\upsilon]^{2}$ (allowed direct band gap energy in eV)
5	3.38	3.54	3.32
6a	3.53	3.55	3.42
6b	3.63	3.60	3.50

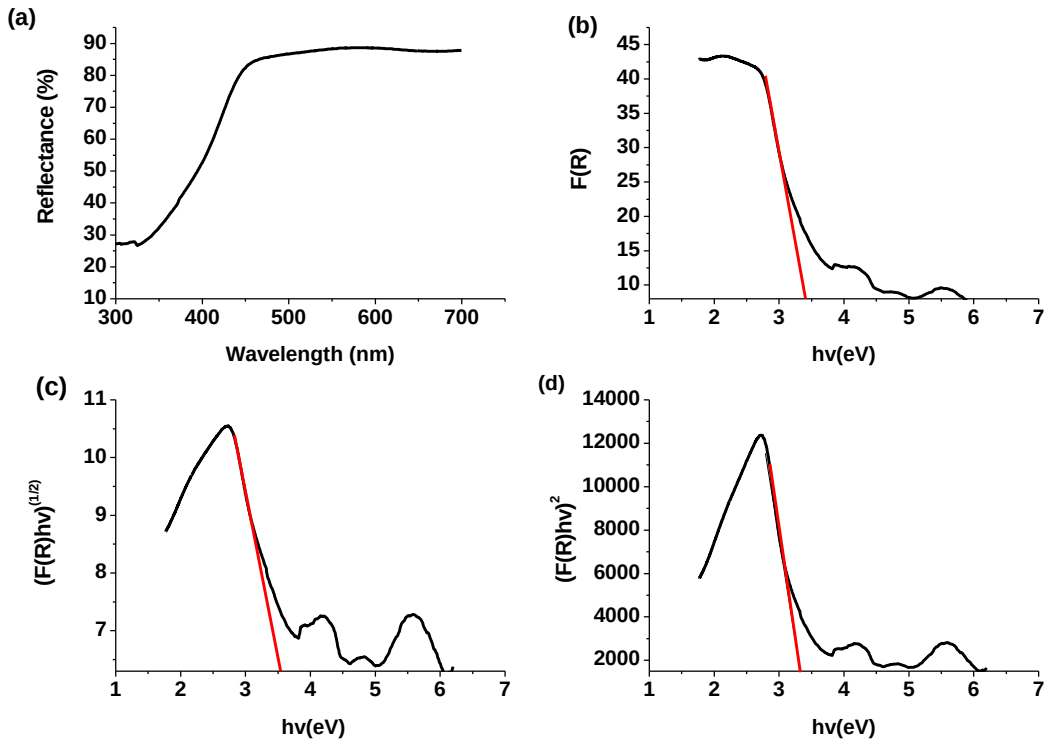

Figure III.25. Plots of (a) Reflectance versus wavelength (b) F(R) versus hυ(eV), (c) $(F(R)h\upsilon)^{1/2}$ versus hυ(eV) and (d) $(F(R)h\upsilon)^{2}$ versus hυ(eV) for **5**.

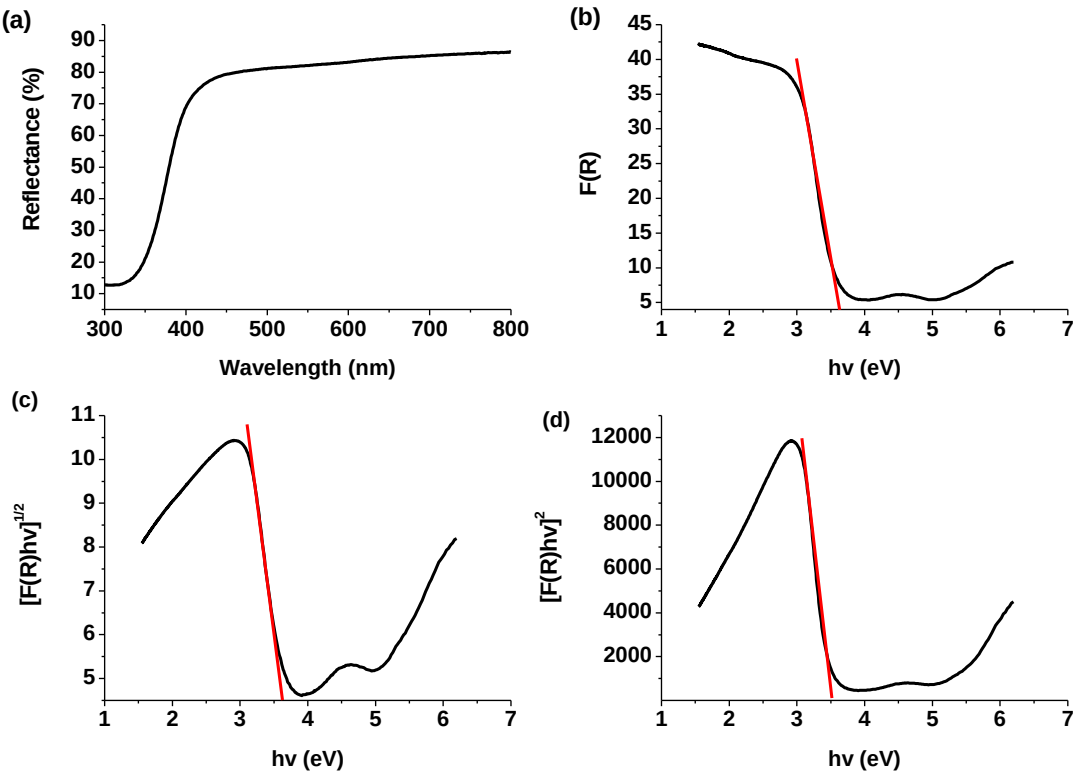

Figure III.26. Plots of (a) Reflectance versus wavelength (b) F(R) versus hυ(eV), (c) $(F(R)h\upsilon)^{1/2}$ versus hυ(eV) and (d) $(F(R)h\upsilon)^2$ versus hυ(eV) for **6b**.

III.3.6. Chemistry of Formation

Self-assembly of solids **3-7** can be visualized in terms of the *supramolecular synthons*: Strandberg cluster, zinc complex, protonated organic moieties and water molecules. pH plays a crucial role in the formation of these synthons. Our previous results have suggested that {P_2Mo_5} cluster is the most stable cluster anion upto pH = 7. Therefore, the formation of Standberg cluster based solids **3-6a** in the present study seems obvious. Since solids **3-6** were synthesized in the pH range 1-5, the ligands exist in their protonated form, which

inhibits their complexation with Zn^{2+} ions in solution (refer Table III.13) and aggregation of supramolecular synthons $(HL)^+$ and $\{H_2P_2Mo_5O_{23}\}^{4-}$ or $\{HP_2Mo_5O_{23}\}^{5-}$ or $\{P_2Mo_5O_{23}\}^{6-}$ is favored.

Table III.13. Ligands and their pK_a values [19].

Sl. No.	Ligand	pK_a
1	benzimidazole	5.4
2	4-aminopyridine	9.17
3	pyrazole	2.5

At pH ~ 2, pyrazole (pK_a = 2.5) can exist in two in ionic forms i.e. {*pz*} ↔ {H*pz*}$^+$. This facilitates the formation of solid **7** as (*pz*) can readily complex with Zn^{2+} centers and (H*pz*)$^+$ can exist as counter cations. On the other hand, 4-*ap* (pK_a = 9.1) is unable to complex with Zn^{2+} ions in solution as it exists in its protonated form in the pH range 1-9. Therefore, **5** and **6a** are formed via aggregation of supramolecular synthons {4-H*ap*}$^+$ and $\{H_2P_2Mo_5O_{23}\}^{4-}$ or $\{HP_2Mo_5O_{23}\}^{5-}$. Interestingly, among the two supramolecular isomers **5** and **6a**, water molecules get incorporated in **5** during aggregation of supramolecular synthons. **5** is crystallized from a more acidic medium as compared to **6a**. Therefore, {P_2Mo_5} cluster anions predominantly exists as $\{H_2P_2Mo_5O_{23}\}^{4-}$. This in turn favors the aggregation of only four {4-H*ap*}$^+$ synthons per $\{H_2P_2Mo_5O_{23}\}^{4-}$ cluster anion. On the contrary, **6a** involves aggregation of five {4-H*ap*}$^+$ synthons per $\{HP_2Mo_5O_{23}\}^{5-}$ cluster anion. Thus, aggregation in the presence of an additional hydrophobic {4-H*ap*}$^+$ synthon perhaps prevents the incorporation of lattice water molecules in **5**. On the basis of above arguments, the self-assembly of {H*bimi*}$_6$[$P_2Mo_5O_{23}$].H_2O (**4**) seems quite reasonable. **4** is crystallized at pH ~ 5

wherein benzimidazole exist as {H*bimi*}$^+$ (pK_a = 5.3). Consequently, it is unable to form complex with Zn^{2+} ions in solution and aggregates with $\{P_2Mo_5O_{23}\}^{6-}$ cluster anions. The high negative charge on {P_2Mo_5} cluster anions favors the aggregation of six {H*bimi*}$^+$ synthons per $\{P_2Mo_5O_{23}\}^{6-}$ cluster anion which in turn restricts the incorporation of large number of lattice water molecules in **4** as compared to **3** due to the high hydrophobicity induced by bulky organic moieties. Therefore, pH dictates the protonation of {P_2Mo_5} cluster anions which in turn influence the aggregation of supramolecular synthons {H*ligand*}$^+$, leading to supramolecular isomers.

III.4. Conclusions

Four new Strandberg cluster based solids were crystallized under hydrothermal condition. Under our reaction conditions, while pyrazole readily formed complex with zinc centers to form a derivatized Strandberg-type cluster *viz.* {H*pz*}$_6${Zn(*pz*)$_4$(H_2O)$_2$} [{Zn(*pz*)$_2$$P_2Mo_5O_{23}$}$_2$].8$H_2O$ (**7**); benzimidazole and 4-aminopyridine formed organic-inorganic hybrid solids {H*bimi*}$_6$[$P_2Mo_5O_{23}$].H_2O (**4**), {4-H*ap*}$_4$[$H_2P_2Mo_5O_{23}$].2H_2O (**5**) and {4-H*ap*}$_5$[$HP_2Mo_5O_{23}$] (**6a**). The occurrence of supramolecular isomerism in the solids **3-6** is driven by pH of the reaction medium. pH directly affects the protonation of the ligands as well as {P_2Mo_5} cluster anion. A careful control of the pH of the reaction medium, inhibits the protonation of {P_2Mo_5} cluster anion which directly affects the {H*ligand*}$^+$:{P_2Mo_5} ratio resulting in supramolecular isomerism. Secondly, formation of water clusters in PMO cluster based solids seems to be dependent on {H*ligand*}$^+$:{P_2Mo_5} ratio. Higher the {H*ligand*}$^+$:{P_2Mo_5} ratio lower is the tendency to form water clusters. The results also suggest that subtle changes in reaction conditions can enable crystallization of new crystalline phases.

From band gap energy calculations two important observations were obtained: (i) the optical band gap energy showed variations when the monoprotonated cluster anion was surrounded by different type of organic ligands and number of water molecules. (ii) band gap energy decreased as the protonation {P_2Mo_5} cluster anion increased, provided the associated organic ligand remained the same.

References

1. Ji, Y. M.; Fang, Y.; Han, P. P.; Li, M. X.; Chen, Q. Q.; Han, Q. X. *Inorg. Chem. Commun*. **2017**, 86, 22-25.
2. Hua, J.; Tian, Y.; Bian, Y.; Zhao, Q.; Zhou, Y.' Ma, X. *SN Appl. Sci.* **2020**, 2, 308-317.
3. Song, L.; Yu, K.; Su, Z.; Wang, C.; Wang, C.; Zhou, B. *J. Coord. Chem*. **2014**, 67, 522-532.
4. Yan, D.; Zheng, L.; Zhang, Z.; Wang, C.; Yuan, Y.; Zhu, D.; Xu, Y. *J. Coord. Chem*. **2010**, 63, 4215-4225.
5. Hu, G.; Dong, Y.; He, X.; Miao, H.; Zhou, S.; Xu, Y. *Inorg. Chem. Commun*. **2015**, 60, 33-36.
6. Asnani, M.; Kumar, D.; Duraisamy, T.; Ramanan, A. *J. Chem. Sci*. **2012**, 124, 1275-1286.
7. Lu, B.; Li, S.; Pan, J.; Zhang, L.; Xin, J.; Chen, Y.; Tan, X. *Inorg. Chem.* **2020**, 59, 1702-1714.
8. Ma, F. X.; Chen, Y. G.; Yang, H. Y.; Dong, X. W.; Jiang, H.; Wang, F.; Li, J. H. *J. Clust. Sci*. **2019**, 30, 123-129.
9. Shi, Z.; Li, F.; Zhao, J.; Yu, X. Y.; Zheng, Y.; Chen, Z.; Guo, Q.; Zhang, G.; Luo, Y. *Inorg. Chem. Commun*. **2019**, 102, 104-107.
10. Wang, Y.; Zhang, L. C.; Zhu, Z. M.; Li, N.; Deng, A. F.; Zheng, S. Y. *Transition Met. Chem*. **2011**, 36, 261-267.
11. Thomas, J. ; Kumar, D. ; Ramanan, A. *Inorg. Chim. Acta* **2013**, 396, 126-135.

12. Zhang, C. X.; Chen, Y. G.; Tang, Q.; Zhang, Z. C.; Liu, D. D.; Meng, H. X. *Inorg. Chem. Commun*. **2012**, 17, 155-158.
13. Moulton, B.; Zaworotko, M. J. *Chem. Rev.* **2001**, 101, 1629-1658.
14. Qu, X.; Feng, H.; Ma, C.; Yang, Y.; Yu, X. *Inorg. Chem. Commun*. **2017**, 81, 22-26.
15. Aranzabe, A.; Wery, A. S. J.; Martin, S.; Gutiérrez-Zorrilla, J, M.; Luque, A.; Martinez-Ripoll, M.; Roman, P. *Inorg. Chim. Acta* **1997**, 225, 35-45.
16. Thomas, J.; Ramanan, A. *Inorg. Chim. Acta* **2011**, 372, 243-249.
17. Brown I D and Altermatt D **1985** Bond-valence parameters obtained from a systematic analysis of the Inorganic Crystal Structure Database *Acta Crystallogr*. **B41** 244.
18. Nakamoto K **1978** Infrared and Raman spectra of inorganic and coordination compounds (New York: John Wiley & Sons).
19. Finar I L **1962** Organic Chemistry, Volume 1 & 2 (London: Longman).